Argonne National Laboratory

REACTOR DEVELOPMENT PROGRAM

PROGRESS REPORT

April 1964

Price $2.00 . *Available from the Office of Technical Services, Department of Commerce, Washington 25, D.C.*

ANL-6885
Reactor Technology
(TID-4500, 29th Ed.)
AEC Research and
Development Report

0543

ARGONNE NATIONAL LABORATORY
9700 South Cass Avenue
Argonne, Illinois 60440

REACTOR DEVELOPMENT PROGRAM PROGRESS REPORT

April 1964

Albert V. Crewe, Laboratory Director
Stephen Lawroski, Associate Laboratory Director

Division	Director
Chemical Engineering	R. C. Vogel
Idaho	M. Novick
Metallurgy	F. G. Foote
Reactor Engineering	L. J. Koch
Reactor Physics	R. Avery
Remote Control	R. C. Goertz

Report Coordinated by
R. M. Adams and A. Glassner

Issued May 15, 1964

Operated by The University of Chicago
under
Contract W-31-109-eng-38
with the
U. S. Atomic Energy Commission

FOREWORD

The Reactor Development Program Progress Report, issued monthly, is intended to be a means of reporting those items of significant technical progress which have occurred in both the specific reactor projects and the general engineering research and development programs. The report is organized in a way which, it is hoped, gives the clearest, most logical over-all view of progress. The budget classification is followed only in broad outline, and no attempt is made to report separately on each sub-activity number. Further, since the intent is to report only items of significant progress, not all activities are reported each month. In order to issue this report as soon as possible after the end of the month editorial work must necessarily be limited. Also, since this is an informal progress report, the results and data presented should be understood to be preliminary and subject to change unless otherwise stated.

The issuance of these reports is not intended to constitute publication in any sense of the word. Final results either will be submitted for publication in regular professional journals or will be published in the form of ANL topical reports.

The last six reports issued in this series are:

October 1963	ANL-6801
November 1963	ANL-6808
December 1963	ANL-6810
January 1964	ANL-6840
February 1964	ANL-6860
March 1964	ANL-6880

TABLE OF CONTENTS

TABLE OF CONTENTS

TABLE OF CONTENTS

TABLE OF CONTENTS

I. BOILING WATER REACTORS

A. BORAX-V

1. Operations and Experiments

Room-temperature, zero-power experiments with the core containing the peripheral superheater, PSH-1, have been completed. The experiments included: neutron flux mapping; determination of the reactivity and power split effects of movement of outside (superheater region) control rods in relation to the remaining control rods; control rod calibration with boric acid; and measurement of boric acid concentration required for reactor shutdown with control rods withdrawn.

At month's end, new, Zircaloy-2, miniature ion chamber thimbles, all in-core instrumentation, and new support brackets had been installed. Preparations for operation at 600 psig and 489°F are essentially complete. Figure 1 shows the location of in-core instrumentation in the PSH-1 core.

a. Reactor Physics. Control rod calibrations using boric acid were made with the superheater steam coolant region drained. With no boric acid, the maximum differential reactivity worth of the 9-rod bank is 1.49%/in. The relative worths of the central rod, four intermediate rods, and four outside rods as percentages of the 9-rod bank are about 29, 57, and 14%, respectively.

Various nuclear parameters measured on core PSH-1 are shown in Table I.

The reactor was found to be subcritical at a concentration of 15.6 g H_3BO_3/gal H_2O with all control rods fully withdrawn at 70°F.

A measurement was made to compare the reactivity effect of various fuel assemblies in core position 35. Compared with water in this location, a boiling fuel assembly containing 39 fuel rods and 12 flow rods is worth 1.33%, a peripheral superheater fuel assembly containing 680 g of U^{235} is worth 1.25%, and a central superheater assembly with 430 g of U^{235} is worth 0.84%.

The effect of boric acid concentration on control rod reactivity worths is being determined. The results of measurements with core PSH-1, shown in Fig. 2, illustrate the relationship between differential control rod worths obtained at various concentrations of boric acid and corresponding critical control rod heights. Here, the 9-control-rod bank differential reactivity worth is compared with the inner 5-rod bank differential worths when the outer control rods are all inserted, all withdrawn, or within the

9-rod bank. The results of measurement of a slight change in boric acid concentration on the reactivity worth of boric acid at near-constant control rod height are illustrated in the 9-control-rod bank data.

No firm conclusions can be drawn from this experiment at this time. Analysis of the data is continuing.

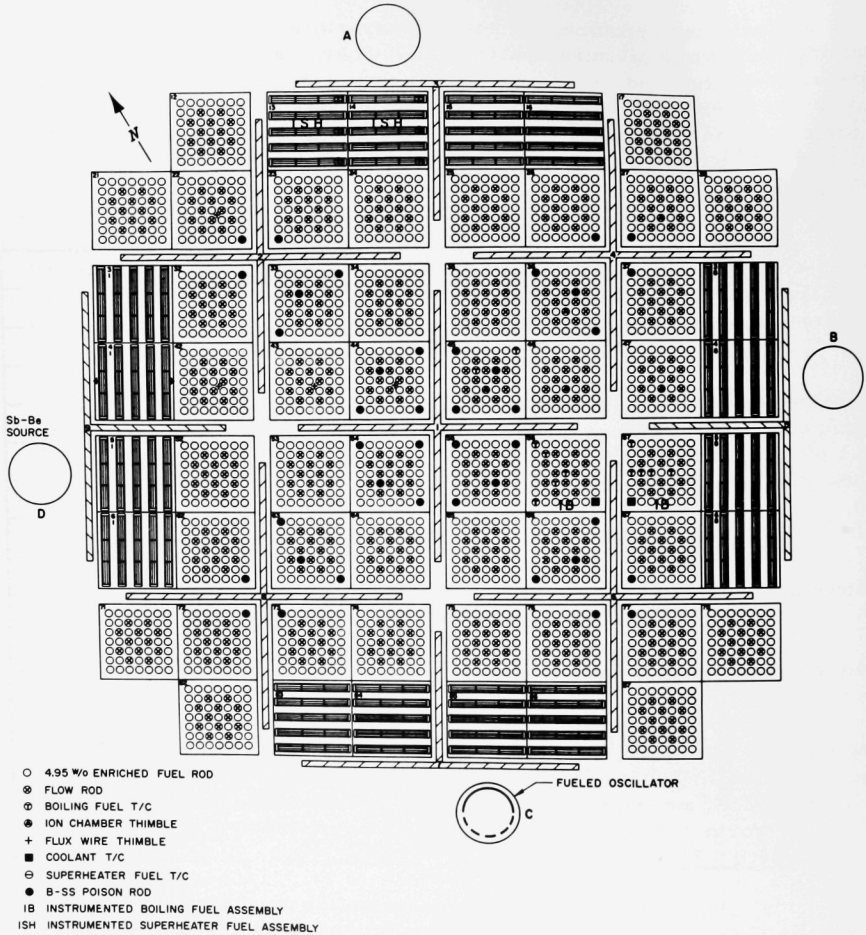

Figure 1. Peripheral Superheater Core PSH-1 of BORAX-V

Table I. Measured Nuclear Characteristics of Core PSH-1 of BORAX-V at Room Temperature

	Reactivity (%)
Available excess reactivity, superheater dry, no boric acid*	+10.5
Shutdown margin, all rods in, superheater dry, no boric acid	~- 8.0
Superheater flooding worths:	
Measured with 9-control-rod bank, no boric acid	+ 1.55
Measured with 9-control-rod bank,* 12.36 g H_3BO_3/gal H_2O in boiler only	+ 1.18
Measured with 5-control-rod bank, outer rods withdrawn, no boric acid	+ 1.88
Boric acid worth, per g H_3BO_3/gal H_2O	~- 0.8

*Uncorrected for effect of boric acid on control rod reactivity worth.

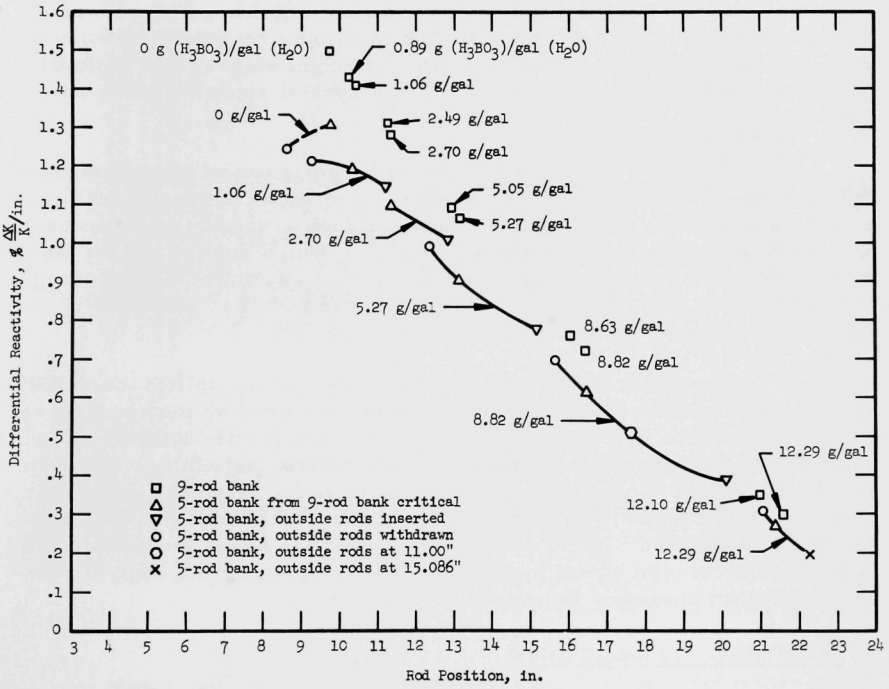

Figure 2. Differential Rod Worth Measurements at 70°F with Superheater Drained for Core PSH-1 of BORAX-V

b. Superheater Flooding Rate. Measurements of superheater flooding rate made with the central superheater core CSH-1, using resistance probes in the fuel assemblies, were not repeated with the peripheral superheater core. However, by flooding over the peripheral superheater inlets at 150 gpm and by visual observation of water rising in all the second-pass superheater fuel assemblies, the highest reactivity addition rate occurs as it did with the central superheater, i.e., the water entering the single short-riser assembly causes the remaining fuel assemblies to fill from the bottom through the flood-and-drain manifold, while the water in the reactor vessel is rising the 2 in. to overflow the standard-height risers of the remaining first-pass assemblies.

During operation with the central superheater core, the time for flooding the fueled region of the 11 standard-riser assemblies was 5.1 sec. Inasmuch as there are 16 superheater assemblies in the peripheral superheater core, flooding of 15 of these 16 assemblies will take a proportionately longer time (6.95 sec). The maximum reactivity addition rate when flooding the peripheral superheater at room temperature is about 0.25%/sec, compared with 0.2%/sec for the central superheater in core CSH-1.

c. Neutron Flux Mapping. Three irradiations at room temperature and zero power were made for fine power mapping of the peripheral superheater core PSH-1. The relative power for each assembly in a representative fraction of the core is indicated in Fig. 3, which shows that the maximum ratio of the power produced in an individual fuel assembly to the average core power is 1.68. About 17% of the total core power is produced in the superheater region, compared with the desired 19%.

The effect on the superheater-boiler power split in core PSH-1 of nonbanked control rod configurations was measured by means of three coarse, radial flux wire irradiations. These configurations were: (1) all nine control rods banked; (2) the four outer control rods fully withdrawn and the inner five banked; and (3) the central rod at 5 in., the outer four rods completely withdrawn, and the four intermediate rods banked. The results are shown in Fig. 4. It appears possible to affect the power split in favor of increased steam temperatures by optimizing the control rod positions when operating at power.

2. Installation and Maintenance

Before being loaded into the reactor, instrumented peripheral superheater fuel assemblies PSI-18 and PSI-19 were reworked as follows: the flexible conduit on all instrument leads was extended 20 in. so that these fuel assemblies might be used at any reactor location. The extension also required splicing extra length on the two Venturi pressure tubes and replacing all Conax pressure seals on the reactor vessel seal plate. Both assemblies were found to be satisfactory upon autoclaving at 600 psig and 489°F. Steam

flow transmitters for the instrumented superheater fuel assemblies have been calibrated to provide a full-scale steam flow indication at 10,000 lb/hr.

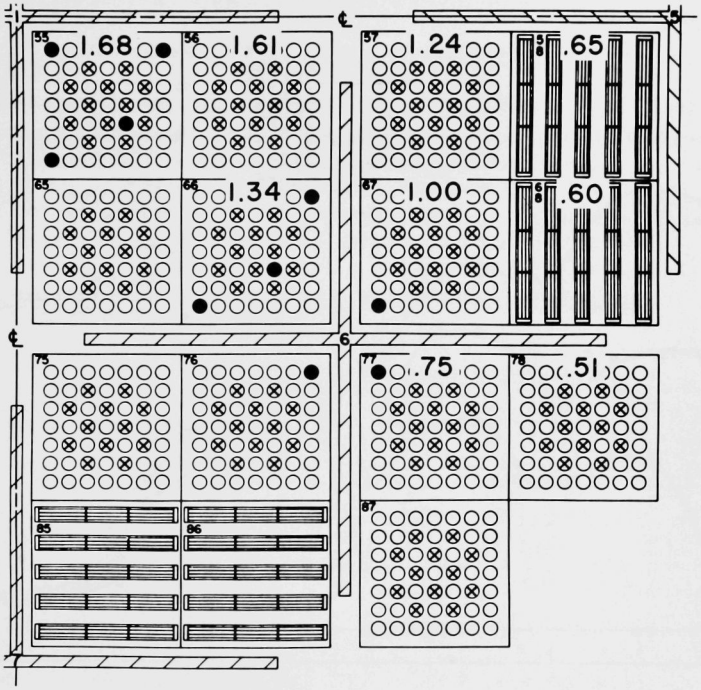

Figure 3. Local-to-core Average Ratio of Power Produced in Individual Fuel Assemblies of Peripheral Superheater Core PSH-1 of BORAX-V

New instrumented boiling fuel assembly I-3 required replacement of its inlet turbine-type flowmeter after an autoclave test caused severe bulging of a liner ring within the meter. The bulged ring caused binding of two turbine blades at their tips and was not immediately repairable. The new meter was autoclaved, and the inlet and outlet meters on the completed fuel assembly were calibrated in the air-water test loop. Instrumented

boiling fuel assembly I-1, which was used in core CSH-1, was found to be satisfactory upon check.

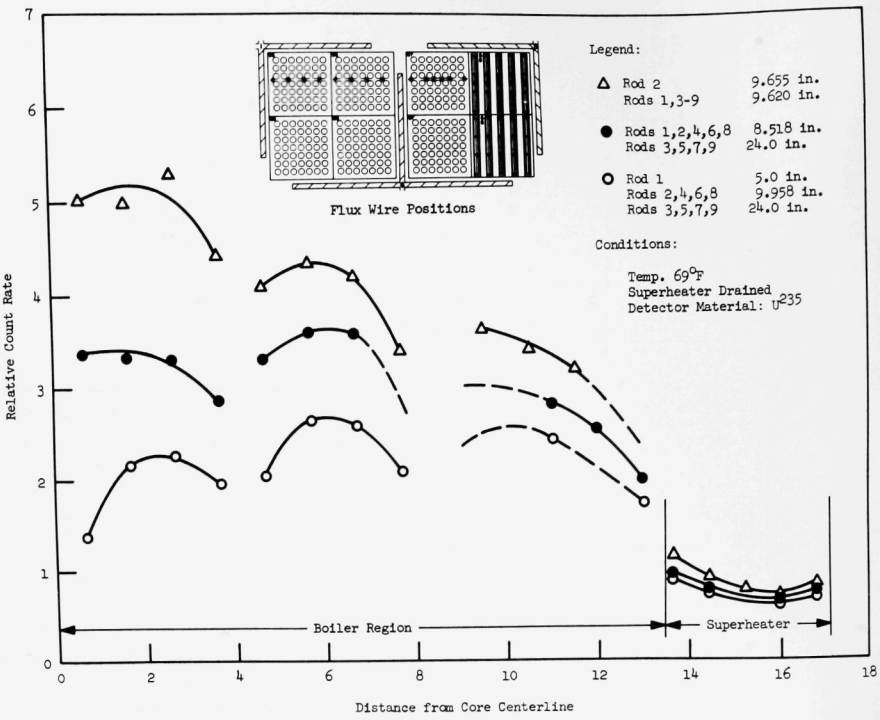

Figure 4. Radial Flux Distribution (Coarse) for Peripheral Superheater Core PSH-1 of BORAX-V

II. LIQUID-METAL-COOLED REACTORS

A. General Fast Reactor Physics

1. ZPR-III

a. RAPSODIE Experiments. Experiments with the RAPSODIE engineering mockup, Assembly 44, during this month were concerned with material reactivity worths and reaction rate distributions.

The reactivity coefficients of sodium as a function of radial and axial positions in the core were determined (see Table II).

Table II. Sodium Worth in RAPSODIE vs. Radial and Axial Location

Axial Region (in. from core center)	Radial Zone Outer Radius: Zone I = 3.1 cm (Ih/kg)	Zone II = 9.4 cm (Ih/kg)	Zone III = 14.3 cm (Ih/kg)	Zone IV = 18.6 cm (Ih/kg)
-1 to +1	-	65	114	104
+1 to +4	85	100	122	125
+4 to +7	175	191	134	118

Central reactivity coefficients were measured in this engineering core configuration as was done with the physics core. A sample-changer mechanism allowed measurements for several materials during the day without separation of the machine halves. Again the sample space was 2 x 2 x 2 in., and each day several references were run with the space void. Differences in reference critical positions were used to evaluate reactivity corrections due to temperature drift. Table III presents the results for sample relative to void. Two different densities were used for steel and aluminum in order to investigate self-shielding effects, but the data show that, to within the accuracy of the measurements, no density effect was present.

Reactivity coefficients for the fissile materials were measured as a function of radial and axial position throughout the core, and in the gaps and blankets. These measurements were made by traversing small samples of the materials (enriched uranium, depleted uranium, and plutonium) along the core axis and radially through the core center. Analyses of these data are in progress.

Similarly, small fission chambers, plated with enriched uranium, depleted uranium, and plutonium, were traversed radially and axially through

the reactor and count rates established at a number of positions. The reaction rate for $B^{10}(n,\alpha)$ was measured at various positions by traversing a small BF_3 chamber.

Table III. Central Reactivity Coefficients in RAPSODIE Engineering Core

Material	Reactivity Coefficient (Ih/kg)
Aluminum, 100 v/o	+11.9
Aluminum, 56 v/o	+11.4
Iron	-5.4
Chromium	+4.4
Nickel	-19.3
Stainless Steel, 100 v/o	-5.1
Stainless Steel, 56 v/o	-5.2
Sodium	+62.0
Oxygen	+60.0

b. Doppler Measurements. The assembly and testing of a number of Doppler fuel elements for use in the ZPR-III facility is progressing. All major design details have been fixed. The natural uranium fuel cans have been filled and are currently being tested for leaks when heated. The solution to the misalignment of the ZPR-III matrix tubes and the elements which may cause binding in the element drives is being studied.

2. ZPR-IX

Assembly No. 3, which is a 7-plate depleted uranium, 7-plate tungsten, and 2-plate enriched uranium assembly, is being completed. This assembly represents the midpoint in a study series of similar assemblies in which the depleted uranium diluent has been gradually replaced by tungsten. In the accompanying analysis, the effect of this tungsten-to-U^{238} interchange upon a range of calculable reactor parameters is investigated. In order to keep the comparison straightforward, identical calculational methods and cross sections are used in all cases.

Part of the results are given in Tables IV and V. In both tables equivalent results for the ZPR-III Assembly No. 22 are included. Except for the small volume fraction taken up by the matrix, the cores of ZPR-III Assembly No. 22 and ZPR-IX Assembly No. 1 are identical. The differences between the two assemblies are almost entirely due to their different reflectors and the corresponding change in core volumes. Assembly No. 22 is reflected by a 30-cm-thick depleted uranium reflector, whereas ZPR-IX Assembly No. 1 is reflected by a 30-cm-thick aluminum reflector.

Table IV. Comparison of Experimental and Calculated Critical Masses

Assembly	Experimental Uncorrected Critical Mass, kg[a]	Experimental Homogeneous and Spherical Critical Mass, kg[b]	Calculated Critical Mass, kg[c]	N^{25} Used in Calculations	Calculated Critical Radius, cm	Calculated Critical Volume, ℓ	Ratio of $\left(\frac{\text{Exp-Calc}}{\text{Calc}}\right)$[d]
ZPR-III No. 22	241	239	278	0.00452	38.6	158	-0.14
ZPR-IX No. 1	278.5	267	332	0.004512	35.7	190	-0.19
ZPR-IX No. 2	383	366	441	0.00451	39.1	251	-0.17
ZPR-IX No. 3	492	474	562	0.004472	42.5	322	-0.16

[a]The experimentally measured cylindrical critical mass corrected only for excess reactivity present in control elements.

[b]Corrected for heterogeneity, core-edge nonuniformity, control gap, and converted to equivalent spherical critical mass by means of shape factors, ~0.92-0.94.

[c]All calculations in spherical geometry by means of the RE-122 diffusion code, cross-section set No. 201, 20-30 mesh points in the core, and tungsten material No. 37.

[d]Exp. refers to the corrected experimental critical mass. Calculated mass is obtained by varying core volume with the experimental core composition. For example, for ZPR-III No. 22, the cited value -0.14 corresponds to $\Delta k/k \approx 0.021$.

Table V. Calculated Kinetics Parameters for ZPR-IX Assemblies

Assembly	Fission Fraction in U^{235}	Fission Fraction in U^{238}	Prompt Neutron Lifetime, sec x 10^8	β_{eff}	Rossi-α, sec^{-1} x 10^{-4}	Average Neutron Delay Time, sec	lh/% Δk	lh/$
ZPR-III No. 22	0.7234	0.2765	6.29	0.00738	11.8	0.0769	469	345
ZPR-IX No. 1	0.7668	0.2332	6.06	0.00728	12.0	0.0768	469	341
ZPR-IX No. 2	0.8283	0.1717	7.39	0.00723	9.78	0.0789	457	330
ZPR-IX No. 3	0.8800	0.1200	8.17	0.00708	8.66	0.0806	446	316

3. Instrumentation Development

a. AFSR. During April, the malfunction of part of the AFSR pneumatic system occurred. In the course of a normal startup, the safety plug, which is raised pneumatically, did not rise off the bottom limit switch. The trouble was traced to leakage in the 4-in.-diameter air cylinder. The piston seal was worn to the point that the air which is used to raise the piston leaked out faster than it was delivered through the $\frac{1}{16}$-in.-ID restrictor tubing. There was no indication that the scram times were affected. Scram-time measurements made a few days before failure of the "air up" system showed no change from previous measurements. The air cylinder was disassembled and the piston seal replaced. Following re-installation, the safety plug alignment and scram time were checked and found to be satisfactory. The reactor was returned to service.

b. Solid-state Neutron Spectrometer. The solid-state fast neutron spectrometer work continued. Data taken at the center of the grazing hole in AFSR was good enough to warrant attempts at "unfolding" the spectrum with machine calculations on the IBM-704.

AFSR was used for the experimental comparison of fission counters from ZPR-III and the UKAEA to obtain a cross-check of fission rate ratios measured by the two groups. Thermal neutron flux intercalibrations of fissile foils were also done. Provisional results indicate no large discrepancies between the weights of fissile materials on the foils as determined radiochemically and by thermal calibration.

B. General Fast Reactor Fuel Development

1. Metallic Fuels

Uranium-plutonium-base alloys are being investigated for use as fertile-fissile fuel materials in fast breeder reactors because many combinations of the base elements, which are readily available, have good neutron yield and breeding ratios. Alloying additions appear necessary, however, to improve the stability of the uranium-plutonium base in a fast-reactor environment and the compatibility of the fertile-fissile alloy with jacketing materials. Fizzium (Fz), which is a relatively high-zirconium combination of desirable fission-product metals retained in the fuel on reprocessing, has good alloying possibilities. The properties and behavior of uranium-plutonium-fizzium (U-Pu-Fz) alloys, as well as various combinations of the constituent elements, are therefore being investigated.

a. U-Pu and U-Pu-Fz

(i) Melting Ranges and Solid Transformations. The melting ranges and the solid transformations of U-10 w/o Pu and U-10 w/o Pu-10 w/o Fz alloys are being determined by thermal analysis. Results to date are compared in Table VI with those obtained from the breaks in heat-content curves (see Progress Report for March 1964, ANL-6880, p. 15). Equivalent U-10 w/o Pu transformation points from the Los Alamos U-Pu phase diagram[1] are also tabulated.

Table VI. Solidus, Liquidus, and Solid Transformation Temperatures of U-10 w/o Pu and U-10 w/o Pu-10 w/o Fz

U-10 w/o Pu	Thermal Analysis (°C)	U-Pu Phase Diagram (°C)
$\alpha \rightarrow \alpha + \beta$		580
$\alpha + \beta \rightarrow \beta$		590
$\beta \rightarrow \beta + \gamma$	735	730
$\beta + \gamma \rightarrow \gamma$		740
Solidus	1025	1030
Liquidus	1060	1080

U-10 w/o Pu-10 w/o Fz	Thermal Analysis (°C)	Calorimetry (°C)
Solid transformations	535	535
	630	600
		660
Solidus	910	900
Liquidus	1010	1030

[1] J. Nuclear Materials 3, 233 (1959).

Recent determinations of the composition of the phases in the U-10 w/o Pu-10 w/o Fz alloy by electron-microprobe analysis have helped to follow the behavior of zirconium in this alloy. The macro and micro compositions are given in Table VII. The as-cast structure is composed of a retained solid solution of uranium with Pu, Mo, Ru, Rh, and Pd in the matrix, and separate U-Zr and U-Pu phases in the boundaries of the gamma grains. After prolonged annealing, some of the ruthenium exchanges with the uranium in the zirconium phase, and hence the grain-boundary phase that was UZr tends to become ZrRu. This is a slow exchange, which is roughly half complete after 60 days at 850°C. The resulting matrix consists of a solid solution of uranium with 7.3 w/o Pu, 2.8 w/o Mo, and 1.7 w/o Ru. It contains essentially no zirconium. A discontinuous grain-boundary phase in the heat-treated structure consists almost entirely of uranium and plutonium in about equal amounts. This composition, according to the binary phase diagram, has a very low melting point and can be expected to drastically influence mechanical properties at elevated temperatures.

Table VII. Macro and Micro Compositions of a Cast and Heat-treated U-10 w/o Pu-10 w/o Fz Alloy

	Specimen Composition (w/o)		Separate Phase Compositions (w/o) (determined by microprobe analyzer)		
Element	Charged	Analyzed	Matrix	Gray on E.B.S.[a]	Black on E.B.S.[a]
U	80.0	80.1	85.5	~40	~18
Pu	10.0	10.0	7.3	~58	~5
Zr	2.75	2.70	0.1	~0.2	~39
Ru	2.95	3.05	1.7	~1.4	~32
Mo	2.80	2.70	2.8	~1.1	~3.6
Rh	0.5	0.48	b	b	b
Pd	1.0	1.01	b	b	b

[a]E.B.S. - electron-back-scatter (image).
[b]Not analyzed.

(ii) Compatibility with Potential Cladding Materials. Currently the behavior of U-10 w/o Pu-10 w/o Fz versus V-20 w/o Ti is being examined. Previous results are given in Progress Report for March 1964, ANL-6880, p. 17. The study is being extended to include 700°C for 9 x 10^6 sec (104 days). The tests of U-10 w/o Pu-10 w/o Fz versus V-10 w/o Ti have been extended to include 9 x 10^6 sec at 650°C. All data to date for penetration of fuel into cladding for these combinations (determined metallographically) are summarized in Figure 5.

Recent microprobe analyses at Mound Laboratory of U-10 w/o Pu-10 w/o Fz/V-10 w/o Ti and U-10 w/o Pu-10 w/o Fz/V-20 w/o Ti diffusion couples indicate that no penetration of U, Pu, Mo, Ru, or Zr into the cladding occurs beyond that seen metallographically.

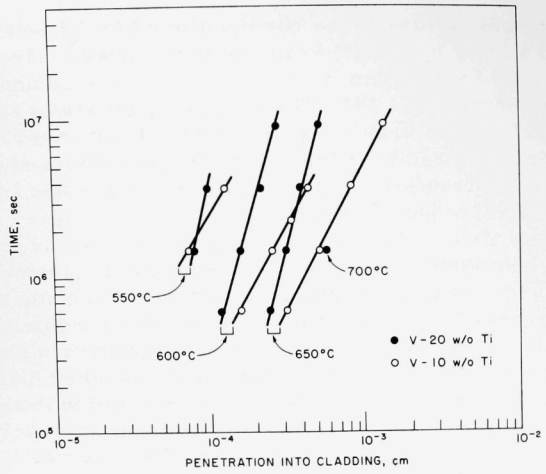

Figure 5

Penetration of V-10 w/o Ti and V-20 w/o Tiby U-10 w/o Pu-10 w/o Fz

2. Development of Jacket Materials

a. Vanadium and Vanadium Alloys. Jacket materials for the fuel elements of fast reactors must have suitable high-temperature properties, including strength and integrity, good thermal conductivity, and compatibility with the nuclear fuel and with liquid-metal coolants such as sodium. The jacket materials must also be amenable to fabrication into the desired shapes. Of the various potential jacketing materials that have been considered, vanadium-base alloys are among the more promising, and titanium is the element favored for use as an alloying element in the vanadium. The optimum titanium content in the alloy is not yet known; for example, the vanadium-titanium alloy that is most inert to sodium is not likely to be the composition that is easiest to fabricate. The properties and fabricability of vanadium and of vanadium-titanium alloys are therefore being investigated.

Results to date indicate that compositions with 10 to 20 w/o of titanium are probably most suitable, but compositions with up to at least 30 w/o are being studied. Alloys with higher percentages of titanium have been made, but their hardness is greater and they are less easy to fabricate.

(i) Fabrication. Investigation of the consolidation and fabrication of a V-20 w/o Ti (TV-20) alloy has continued.

A second 9.7-cm (3.8-in.)-diameter ingot (AM25) of TV-20 alloy has been cast by the consumable-arc process during the month. The titanium analysis is 19.7 ± 0.4 w/o. Following X-ray inspection, the arc-cast ingot was cropped and machined to a 8.9-cm (3.5-in.)-diameter extrusion billet weighing approximately 13.5 kg. Ultrasonic inspection of the

machined billet revealed no internal defects, and the billet was extruded to provide stock for re-extrusion into sheet bars and tube blanks.

The TV-20 tube blanks that were extruded last month (see Progress Report for March 1964, ANL-6880, p. 19) have been pickled in hot HCl to remove the Type 304 stainless steel cladding from the inner and outer surfaces. The dejacketed surfaces were so good that there was no need for conditioning before secondary fabrication.

Sections of the tube-blank stock, 1.69-cm OD x 1.16-cm ID (0.665-in. OD x 0.456-in. ID) of varying lengths, were swaged over a hardened steel mandrel to 1.45-cm OD x 1.15-cm ID (0.573-in. OD x 0.453-in. ID) and vacuum-annealed for 1 hour at 900°C. A hard-drawn copper core was then inserted into the tube and the composite rod was drawn to about a 70% reduction in area. The TV-20 tube was lifted off the copper core with a light swaging pass. After core removal the tube measured approximately 0.83-cm OD x 0.67-cm ID (0.328-in. OD x 0.266-in. ID). The tube was again annealed for 1 hour at 900°C after which an annealed copper core was reinserted and drawing was continued to near the final size. The copper core was removed, and the tube was cleaned and finished to final size by drawing over a hardened steel mandrel. "Teflon" was used as the lubricant for all drawing operations.

The TV-20 alloy is quite amenable to cold working by drawing, swaging, or rolling; but the alloy has a marked propensity for galling during drawing and all dies must be in perfect condition to prevent longitudinal striations and/or surface pickup.

b. Molybdenum Alloys

(i) High-temperature Mechanical Properties. The errors reported in determining the elastic modulus with a high-temperature mechanical extensometer (see Progress Report for March 1964, ANL-6880, p. 21) have been attributed to a fractured member in the linkage of the extensometer. After the linkage was repaired, the modulus was measured for Mo-0.5 w/o Ti-0.08 w/o Zr (TZM) at room temperature and at 650°C. The modulus was also measured at room temperature with a clamp-on extensometer. The room-temperature values for the elastic modulus are reported in Table VIII.

Specimens machined from a new shipment of TZM exhibited significantly greater strength than previously reported (see Table IX).

Table VIII. Room-temperature Elastic Modulus of Mo-0.5 w/o Ti-0.08 w/o Zr (TZM)

Specimen Number	Strain Magnification	Number of Trials	Elastic Modulus (10^3 kg mm^{-2})
	Clamp-on Extensometer		
1	500X	7	$34.6^{+5.2}_{-2.0}$
	1000X	10	$32.8^{+2.2}_{-1.5}$
	500X	7	$31.3^{+6.5}_{-0.1}$
2	500X	12	$31.0^{+0.4}_{-0.7}$
	1000X	12	$31.2^{+0.2}_{-0.8}$
	High-temperature Mechanical Extensometer		
1	400X	10	$33.2^{+0.8}_{-1.5}$

Table IX. Tensile Properties of Mo-0.5 w/o Ti-0.08 w/o Zr at 650°C for Two Lots of Material

Ultimate Tensile Stress (kg mm^{-2})	Yield Stress (kg mm^{-2})	Elongation (%)	Reduction of Area (%)	Elastic Modulus* (10^3 kg mm^{-2})
		Lot 1		
56.0	49.1	23	86	
57.4	55.0	22	89	
55.7	55.0	>17.7	85	
		Lot 2		
68.8	66.0	19	84	30.4
70.1	69.0	21	86	23.9
72.4	72.4	>19	>82	25.0
74.9	72.1	22	87	22.8
				Average = $25.5^{+4.9}_{-2.7}$

*Strain rate, 2.1×10^{-4} sec^{-1}.

3. Zero Power Reactor Fuels

a. Properties of Zero Power U-Pu-base Fuel Alloys. The program to develop a U-Pu-base metal fuel for zero power critical studies is continuing (see Monthly Progress Reports for September and November 1963, and March 1964). Recent emphasis has shifted to somewhat lower plutonium contents (~20%).

Recent results for corrosion by room air of binary U-Pu, U-Pu-Fe, and U-Pu-Mo alloys are summarized in Table X.

Table X. Corrosion of U-Pu-base Alloys in Air

Specimen No.	Alloy (a/o)	Casting Method	Length of Test, Days	% Weight Gain	Remarks
10	$(U_{0.82}Pu_{0.18})_6Fe$	Injection cast	45	1.9	Very slightly tarnished. Weight nearly constant after 14 days.
11	U-27 Pu-6 Mo	Injection cast	35	0.2	Has very thin black film.
12	U-27 Pu-6 Fe	Injection cast	35	7.0	Began disintegrating on 10th day. Completely disintegrated by 12th day.
13	$(U_{0.82}Pu_{0.18})_6Fe$	Injection cast	35	0.1	From same casting as specimen No. 10, except cast surface machined off. Very slightly tarnished. Weight nearly constant after 14 days.
14	$(U_{0.82}Pu_{0.18})_6Fe$	Chill cast as 9.02-cm-thick plate	35	1.1	Very slightly tarnished. Weight nearly constant after 14 days.
15	$(U_{0.82}Pu_{0.18})_6Fe$	Chill cast as 2.21-cm-thick plate	31	0.7	Very slightly tarnished. Weight constant after 10 days.
16	$(U_{0.82}Pu_{0.18})_6Fe$	Chill cast as 4.57-cm-thick plate	31	0.6	Very slightly tarnished. Weight constant after 10 days. Developed several cracks after 19 days.
17	U-18 Pu	Injection cast	31	0.4	Blackened, swollen, and cracked in 17 days.
18	U-18 Pu	Cast into 270°C mold	18	0.1	Surface blackened in 8 days. Began to swell and disintegrate by 18th day.
19	U-18 Pu	Chill cast	14		Surface nearly all black by 14th day.

Several elements have been tried as alloying additions to the pyrophoric U-Pu alloys in an effort to improve their corrosion resistance. Early air-corrosion and ignition-test results indicated that either iron or molybdenum gave the desired results. Iron was favored as being the least undesirable from physics considerations. However, further studies showed that the corrosion resistance and the structure of a U-27 a/o Pu-6 a/o Fe alloy were extremely sensitive to the method of casting and appeared to deteriorate with time. Injection-cast (coarse-grained) material had a relatively low ignition temperature and completely disintegrated in a 12-day exposure to flowing room air (see Specimen 12 in Table X). However, a chill-cast (fine-grained) alloy of the same composition had a very high ignition temperature and began to show appreciable corrosion only after 11 weeks under similar conditions. Also, the ignition temperature of the chill-cast material was much lower after several months of storage than when tested soon after casting.

Both iron and molybdenum additions have been tried as part of the SEFOR zero-power fuel studies.

Early indications were that 18% Pu would satisfy the SEFOR requirements. The maximum solubility of plutonium in alpha uranium is very close to this. An attempt to eliminate the detrimental zeta phase by heat treating the U-18 Pu binary alloy was unsuccessful. A later increase of the plutonium requirement to 20% made this approach even less attractive.

Another way to eliminate the zeta phase would be to add sufficient iron (3.77 w/o) to get single phase $(U_{0.82}Pu_{0.18})_6Fe$. All efforts to make sound crack-free castings of this composition have failed. However, the corrosion resistance of this material appears to be satisfactory (see Table X).

The molybdenum alloys have by far the best combination of properties. They are easy to cast and machine, have good room-temperature resistance to air corrosion, and have high ignition temperatures. Tests of the U-27 a/o Pu-6 a/o Mo alloy indicate that its pertinent properties are relatively insensitive to the casting method, and it does not deteriorate with time.

We are now trying to determine the minimum amount of molybdenum necessary to give the desired properties in the SEFOR alloy. U-20 a/o Pu alloys containing 4.5 a/o Mo and 3 a/o Mo are being evaluated. Also vanadium and titanium are being examined as potential alloying elements.

C. General Fast Reactor Fuel Reprocessing Development

1. Skull Oxidation

The skull material remaining in a zirconia crucible after pouring of melt-refined EBR-II fuel alloy is transformed to an easily pourable powder by oxidation preparatory to recovery of the uranium by the skull reclamation process. During oxidation, some of the zirconia crucible materials may slough off into the skull oxide. Samples of oxidized skull material obtained in six runs in which uranium-fissium-0.65% cerium charges were melt refined in separate crucibles have been analyzed for zirconium. Analytical results indicated that zirconium from crucible fragments constituted only 1.3 w/o of the skull oxide. This amount would cause no problems in the skull reclamation process.

2. Skull Reclamation Process

Engineering-scale (1.5 kg of uranium) runs are being made in order to establish mechanical reliability of equipment and to develop operating techniques for the recovery of uranium (see Progress Report for November 1963, ANL-6808, p. 24) from oxidized melt-refining skulls. Following each step in the skull reclamation process, an impurity-bearing salt or metal phase is separated as completely as possible from a uranium-bearing phase.

During the past month, two engineering-scale skull reclamation runs were carried out without shutdowns between steps. The waste impurity solutions were removed with efficiencies of 88 to 96%, more than adequate for process requirements.

The waste metal solutions are each removed from beneath a solidified salt layer. During intervals when the crucible contents are being cooled to solidify the salt layer prior to the transfer of a molten metal phase, the agitator is slowly rotated to maintain a path (through the salt) for pressurizing gas which subsequently forces the metal out of the crucible and into a waste container. Before the second of the engineering-scale runs, the round agitator shaft was machined to a hexagonal shape to provide a larger path for the pressurizing gas. By means of this modification, the gas pressure required to effect transfer was reduced from the range of 15 to 20 psi to between 4 and 8 psi.

3. Materials and Equipment Evaluations

A 4-in.-OD, 6-in.-high tungsten crucible (see Progress Report for March 1964, ANL-6880, p. 31), which had been fabricated by spinning from a tungsten sheet, successfully withstood 14 cycles of heating to 800°C and cooling to room temperature while charged with 835 g of 50 w/o zinc-magnesium and 417.5 g of flux. The crucible contents were molten and frozen at the two temperature extremes. On the basis of the good performance of the spun crucible and a lower quoted price for a full-scale spun crucible than for full-scale crucibles fabricated by several other techniques, bids have been requested for a 10-in.-OD, 20-in.-high spun crucible with baffles.

4. Advanced Processes

Work has continued on the development of liquid metal processes for the recovery of plutonium and uranium from fast power reactor fuels. In the process flowsheets currently under study, basic separations of fission products from uranium and plutonium are effected by equilibration of the fuel constituents between liquid metal and molten salt solvents.

The cadmium-zinc-magnesium system is being considered for use as a process solvent because of its low corrosion rates in stainless steel and the possibility of operation at relatively low temperatures. Uranium solubility data were obtained earlier in a set of experiments, using cadmium concentrations of 50 to 84 a/o, zinc concentrations of 6 to 30 a/o, and magnesium concentrations of 10 to 20 a/o (see Progress Report for January 1964, ANL-6840, p. 31). The intermetallic uranium compounds in equilibrium with the saturated solution in this general region of composition have been identified. X-ray results, chemical analysis, and electron probe microanalysis of crystals in quenched samples (from the intermediate temperature region of about 450 to 600°C) show that the delta-phase compound,

U_2Zn_{17}, is in equilibrium with the saturated solution. However, with increasing cadmium concentration in the solvent, increasing amounts of cadmium substitutes for zinc in the U_2Zn_{17} lattice. Cadmium concentration in the crystals ranges from about 3 to 4 a/o when the cadmium concentration in the solvent is 60 to 70 a/o, and from about 5 to 7 a/o when there is 75 to 80 a/o cadmium in the solvent. A similar quenching experiment with a Cd-Zn-Mg solution saturated with plutonium has been performed, but definitive results are not yet available.

D. Sodium Coolant Chemistry

Impurities in sodium used as a coolant in reactors may result from reaction of sodium with contaminants in the cover gas. To determine the importance of this source, reactions of sodium with various gases which might be contaminants are being investigated. Initial experiments have been performed with distilled sodium and carbon monoxide (at pressures below ~9 mm) to measure the effects of temperature and gas pressure on reaction rate. Preliminary results at an initial carbon monoxide pressure of about 2.5 mm indicate no reaction (i.e., absence of pressure change) below 289°C and a constant reaction rate in the temperature range from 304 to 340°C. The reaction rate appears to be approximately second order with respect to the carbon monoxide pressure.

The solubility of carbon in sodium has been measured at 250°C. The sodium contained about 100 ppm oxygen and thus probably was saturated with respect to sodium oxide. A tentative value of 33 ppm carbon was obtained. This agrees fairly well with the value obtained by Gratton,[2] namely, about 42 ppm at an oxygen concentration of approximately 40 ppm.

E. EBR-I

Unloading of plutonium Mark-IV fuel rods from EBR-I was completed. A total of 319 rods were shipped to Phillips Petroleum Co. for storage at the Chemical Processing Plant. Four rods are being held for shipment to Hanford for metallurgical examination. An additional 96 rods, never used in the reactor, are awaiting disposal.

The twelve blanket subassemblies were also removed from the reactor and are being stored at the EBR-I facility. One of these contained an antimony source that had become stuck several months previously. The beryllium thimble and source were removed as a unit and stored. The active portion of the Mark-IV fuel subassembly boxes, along with portions of the top unirradiated ends, were sent to Argonne, Illinois, for metallurgical study.

---

[2] J. G. Gratton, KAPL-1807 (1957).

The reactor top cover and shielding were replaced, NaK coolant was transferred from the drain tank to the gravity tank, and the reactor tank was flushed. With the outer blanket elevator raised, the safety and control rod drives were removed in preparation for removal of the control and safety rods. Likewise, the air cylinder for the safety plug was removed in preparation for removal of the plug. All Mark-IV steel dummy rods used during the approach to critical have been disposed of by burial.

F. EBR-II

1. Reactor Plant

During the month, the temperature of the primary system bulk sodium was lowered to about 350°F before filling the secondary system. Combined operation of the primary and secondary systems at 350°F began on April 9, and heating of the combined systems to 590°F followed. Unloading of filter and verification subassemblies from the reactor grid was then accomplished.

a. Primary Sodium Pumps. Checkout of the primary sodium pumps is essentially complete. During most of the heatup of the primary tank bulk sodium from 350 to 590°F, the pumps were operated at about 74% flow. The pumps were operated at full flow for about 42 hr during the cleanliness verification run, and also during measurement of the drop-time characteristics of the control rods.

b. Fuel Handling. Removal of four natural uranium verification subassemblies, two filters, and an enriched core, inner blanket, and outer blanket subassembly from the reactor grid was accomplished. The two filters were removed directly from the primary tank and the sodium distilled from them. With one exception, the other subassemblies were placed temporarily in the storage basket and then removed from the primary tank.

During the removal of the third natural uranium verification subassembly from the storage basket, the subassembly was inadvertently dropped. An investigation indicates that the transfer arm very likely was locked with the subassembly outside the locking pin. It was later demonstrated that the transfer arm could support a dummy subassembly outside the locking pin as the transfer arm was moved vertically with respect to the storage basket.

Using a dummy subassembly, it was determined that the basket position formerly occupied by the "lost" subassembly as well as the only empty adjacent basket position were both empty and the key bars were intact. The path the subassembly travels on the transfer arm between the pre-transfer position and the reactor cover (which was down at the time the subassembly was dropped) was found to be unobstructed.

Manual rotation of the storage basket with the dummy subassembly held in the transfer arm close to the basket indicated no interferences. Such interference should exist if the subassembly is lodged across the top of the storage basket. Manual rotation of the basket in the "down" position also indicated no excessive torque. It appears that the "lost" subassembly fell to the bottom of the primary tank, either into or adjacent to the catch basin. A study of the measures necessary to prevent a recurrence of this incident is under way.

c. Subassembly Examination. The two filter subassemblies, a core and inner blanket type, were opened and examined after sodium distillation. Milligram quantities of black material were found with small quantities of white sodium oxide. About eight small pieces of metallic material were found in the form of small chips. The largest piece was about $\frac{1}{4}$ in. long, 0.010 in. thick, and $\frac{1}{16}$ in. wide. Examination of two verification subassemblies is being performed in ANL-Illinois. The enriched core subassembly will be disassembled and inspected in the Fuel Cycle Facility.

d. Oscillator. The oscillator rod drive was connected, and the rod was oscillated over the design range of reciprocating frequencies and variable stroke lengths. Operation was satisfactory.

e. Control and Safety Rods. The drop time characteristics of control and safety rods under full flow conditions were investigated. Control rods No. 2 and No. 5 were selected as representative, and both rods were tested individually at both zero flow (for comparison with earlier data) and full flow. All eleven rods were also dropped simultaneously, with control rod No. 5 as the instrumented rod. All tests were conducted with a scram assist air pressure of 30 psig. Testing of the safety rods was also scheduled to be completed before the end of the month.

The following represents preliminary information:

(1) The results for zero flow compare favorably with those obtained earlier, except in the dashpot region. Snubbing action is now somewhat faster - apparently as a result of recent modifications. The present behavior appears to be satisfactory, and there has been no significant change to maximum rod acceleration.

(2) Full reactor flow causes some retardation of the rod drop, reducing the maximum acceleration for individual rods from approximately 1.48 g to 1.3 g. Drop time for 10-in. travel is of the order of 230 msec - approximately 20 to 25 msec longer than for zero flow.

f. Rotating Plug Seals. One burned-out seal heater was replaced.

g. Sodium-purification System. The system is now in operation at reduced flow. A faulty copper bus bar joint for the EM pump, which prevented pump operation, was repaired. A thermal air switch in the pump rectifier cooling system was also repaired.

h. Fuel-unloading Machine. Rework (see Progress Report for March 1964, ANL-6880, p. 33) was completed, except for wiring installation for the new inlet line heater and insulation of the associated piping.

i. Fuel-element-rupture-detection Loop (Delayed-neutron Monitor). Installation of heaters and thermocouples was completed. Insulation of the piping loop has begun. Construction of the lead brick shielding wall around the installation is partially complete.

j. Shutdown Coolers. Heat balance tests of the shutdown coolers showed that the cooling air louvers and actuators operated satisfactorily.

k. Reactor Building Containment. A new valve seal has been installed in the purge exhaust isolation valve. The valve has been leak-tested and meets the requirements.

The leak rate of the reactor building freight door was found to be approximately 2 $ft^3/24$ hr.

The two flexible seals for the 12-in.-diameter secondary sodium piping penetrations through the reactor building were leak rate tested. Each unit was pressurized with air at 24 psig for 8 hr, and leak rate was acceptable.

l. Reactor Building Crane. The installed reactor crane interlock has been checked out except for a swinging load test. The interlock prevents crane operation in the area of the control rod cluster during reactor operation.

2. Sodium Boiler Plant

A cross connection between the boiler feed line and the blowdown line was made. Radiography disclosed acceptable welds, and the piping was tested hydrostatically to design specifications. This new line will permit circulation of water through the yard lines during standby conditions to prevent freezing in cold weather.

The temporary cold trap was operated, circulating sodium from one end of the storage tank to the other. Heatup of the secondary sodium system and steam system prior to filling was then started on Tuesday, April 7. The two systems reached the filling temperature of 350°F late on Wednesday, April 8. The secondary system was then filled with sodium, and

combined operation of the primary and secondary systems at 350°F was effected on April 9. Heatup of the combined systems (primary, secondary, and steam) was started at this time and carried out through April 15, when plant standby conditions were achieved (575°F). The plugging temperature of the secondary sodium was maintained below 300°F by operation of the temporary cold trap.

Shortly after plant standby conditions were attained, the leak detector in the outer case of the main secondary EM pump gave an indication of sodium therein. The pump was shut off, and visual inspection confirmed the presence of sodium in the pump case. The sodium was drained to the storage tank, and the piping systems were cooled to room temperature. The steam generator was placed in wet layup, and the sodium-storage tank temperature was reduced to 350°F, where it was maintained.

Electrical tests showed that the resistance heaters in the bottom of the pump case were shorted out. "Megger" tests of the pump windings show them to be unaffected at this time. Attachments such as cooling water lines, argon lines, and electrical connections, were removed from the pump in preparation for removal of the top case section to permit detailed inspection of the pump duct.

Two vendor's representatives inspected the pump. The cover, with attached upper coil winding, was removed. The upper surface of the pump tube was then visible, and two cracks about 2 in. long were found. Evidence of two smaller cracks in the same vicinity was noted. These cracks were near the suction end of the pump and not in the vicinity of the tube welds. The sodium which had leaked was apparently pumped toward the high pressure end of the pump until it hit a baffle at the high-pressure transition and then sprayed sideways. There is no explanation at present as to the cause or origin of these cracks.

The pump tube and lower coil winding are being removed by cutting the 12-in. secondary sodium pipes adjacent to the pump case. It is possible that the repairs can be effected in Idaho. However, if the pump must be returned to the vendor it may take as much as six months for repair. Plans are being made to use a smaller, experimental pump in the meantime if necessary.

The gas chromatograph, which analyzes the argon cover gas for hydrogen, was checked out and placed in operation by a manufacturer's representative. The nitrogen and hydrogen concentrations in the cover gas were high, being 4000 ppm and 2000 ppm, respectively, probably due to air and moisture contamination during the yard welding which connected the secondary piping to the primary heat exchanger.

3. Power Plant

Operations preparatory to approach-to-power were successfully carried out until failure of the secondary sodium pump (see Sect. 2 above).

Preparations were completed for measuring Power Plant high-pressure steam-line movement and expansion from the cold to hot condition; initial readings at the cold condition were taken at eleven points on the piping. Hot readings must await the generation of superheated steam.

During heatup and standby operation, standard operating procedures as given in the EBR-II Operating Instructions, were followed except as modified by interim special instructions. Necessary changes based upon experience during heatup and standby operation will be incorporated in the Operating Instructions. Water was heated in the No. 2 feedwater heater and circulated by the startup feedwater pump. The standby condition of 1250-psi drum pressure was attained, and feedwater and blowdown were circulated at the rate of 8,000 lb/hr, with the excess output bypassed to the No. 2 heater via the warmup line of the motor-driven feed pump.

At plant standby, feedwater was pumped at the rate of 4,000 to 5,000 lb/hr with no blowdown. Steam was dumped to the condenser via the bypass system and desuperheater.

Difficulties were experienced with one of the control valves which bypass steam from the steam main to the condenser. Modifications to improve performance will be effected prior to the next plant startup.

With shutdown of the secondary system, the steam generator was put in wet layup completely filled with water containing 150 ppm of sulfite and sufficient morpholine for a pH of 10.2.

4. Fuel Cycle Facility

a. Removal of Nitrogen from Argon. The removal of nitrogen from argon by gettering the nitrogen on hot (~900°C) titanium sponge is under study because of a possible future need to remove nitrogen from the argon atmosphere in the Argon Cell of the EBR-II Fuel Cycle Facility.

A pilot plant (see Figure 6) has been constructed to obtain information on component reliability. An argon-nitrogen gas mixture is circulated from a surge tank by means of a blower. The flow rate is measured by an orifice meter and manometer. Flow rate is controlled by adjustment of the blower speed in conjunction with a flow-control valve.

The gas passes through a 4-way valve into a regenerative pebble-bed heat exchanger, and into a trickle heater to bring its temperature to the desired 900°C for reaction. All vessels above the dashed line

in Figure 6 are located in a resistance furnace. The titanium bed is maintained at 900°C for reaction of the nitrogen content of argon to titanium nitride. The purified gas passes into a second trickle heater and into a second regenerative heat exchanger. During this part of the cycle, the temperature of the second regenerative heat exchanger slowly rises as heat from the gas is stored. The gas then passes through the 4-way valve, into a heat exchanger to reduce its temperature to room temperature, and into the surge tank. The 4-way valve may be operated on a time cycle so that, at a predetermined time, the valve changes position, reversing the direction of flow through the purification system. This is done to re-use the heat stored in the pebble-bed regenerative heat exchangers. In each part of the cycle, the trickle heater on the inlet side of the titanium reactor is on, and the trickle heater on the downstream side is off. Makeup argon and nitrogen are added to the surge tank.

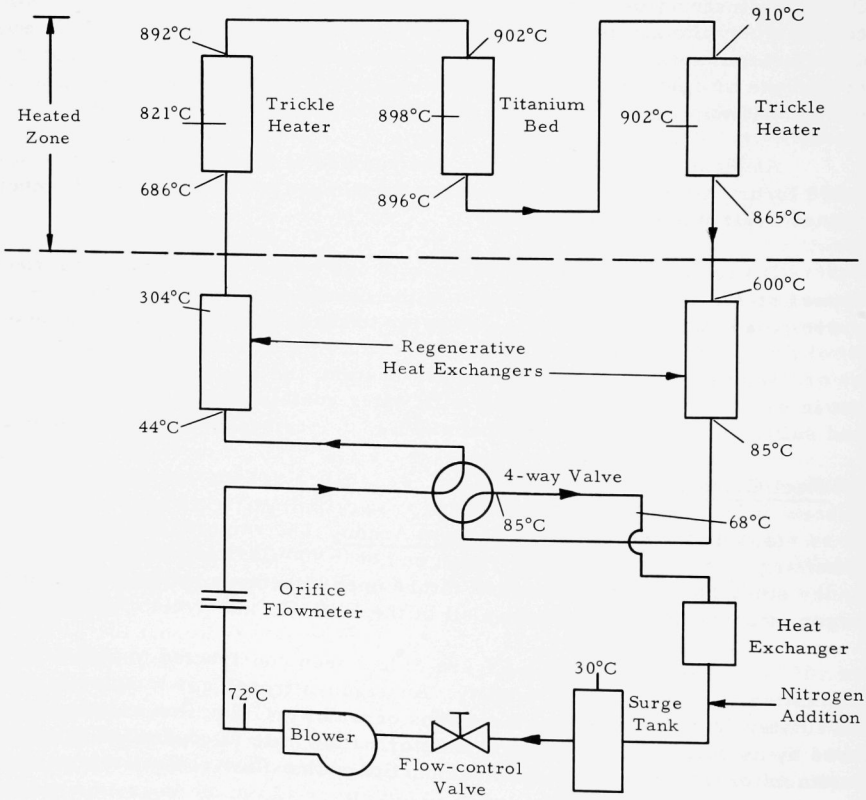

Figure 6. Schematic Diagram of the Pilot Plant Unit for the Removal of Nitrogen from Argon (Approximate temperatures prevailing throughout the system at the completion of a flow cycle are given.)

The pilot plant has been operated continuously for 1000 hr at a gas-circulation rate of 9.2 cfm. All components and instrumentation performed their design functions well. During this long-term reliability run, the system successfully demonstrated the feasibility of large-scale removal of nitrogen from argon by hot titanium sponge. Nitrogen, which was added to the circulating argon at a rate calculated to maintain its concentration at about 650 ppm, was removed at approximately the nitrogen-addition rate during the first 120 hr, during which time an estimated 20% of the titanium sponge was converted to nitride. The nitrogen concentration in the gas reached about 12% after 144 hr of operation; 22 additional hr of operation without nitrogen input then reduced the nitrogen concentration below the limits of detection.

After some 400 hr of operation since the EBR-II Argon Cell was filled with argon (see Progress Report for March 1964, ANL-6880, p. 36), the argon purification compressor and motor were removed from their enclosure for inspection to determine the cause of an increase in bearing noise level and an excessive rise in bearing operating temperature (see Progress Report for March 1963, ANL-6705, p. 22). The examination showed that misalignment of the shafts of the compressor and motor was responsible. To prevent future changes in shaft alignment, the compressor and motor have been dowel pinned to the main base frame. Since this modification, the compressor and motor have been operating satisfactorily.

To eliminate the possibility of mechanical stresses taking place in the in-cell crane-drive machinery, which could result from rapid reversal of the crane motors, anti-plugging relays, which assure that a motor cannot be reversed before it has stopped, have been installed in the crane control cabinets.

The electrical circuitry of the electromechanical manipulators has been modified to prevent simultaneous operation of the arm-rotation motor and the hoist motor. This change will prevent twisting of the hoist cable and will minimize the possibility of arcing in associated electrical connectors and wiring.

The furnace and associated supporting equipment for the oxidation of the residue (skull) remaining in the crucible after melt refining have been installed in the Fuel Cycle Facility (see Progress Report for February 1964, ANL-6860, p. 28).

b. Waste Disposal. High-level activity wastes produced in process operations will be packaged in a waste disposal container (steel pails, $11\frac{1}{2}$ in. in diameter by 6 ft long) before disposal to a waste burial and storage area. The disposal container will serve to hold either 120 lb of subassembly stainless steel waste (from dismantling-machine operations) which has been placed directly in it or 120 lb of waste material which has been previously

packaged in 6 smaller sized (3-gal) capped pails. The 6-ft-long disposal container will be loaded and capped in the Air Cell, and then lowered through a floor plug in the Air Cell into a coffin for transfer to the burial ground. (Detailed drawings are being prepared for fabrication of the transfer coffin for these disposal containers.) At the burial ground, the waste disposal container will be dropped into a lined hole which will then be backfilled with a minimum of 6 ft of dirt. Steel-lined holes will be used for disposal containers which contain radioactive material which will remain hazardous for over 5 years. After the hole is backfilled, the liner will then be sealed by welding on a steel cover.

Impact tests were performed to determine if the drops, which may be as great at 15 ft, would damage a loaded and capped disposal container. In all tests, the same disposal container and cover were used. In one set of tests, the test load in the capped disposal container consisted of 6 three-gal capped pails, each filled with about 20 lb of steel shot. In another set of tests, the test load in the capped disposal container consisted of 120 lb of steel bars, loaded directly into the disposal container. Since the drops in the two sets of impact tests did not loosen the cover or rupture the waste container, the results would indicate that a disposal container used for the first time will not be damaged and the cover will remain tight when the container is dropped into a lined hole.

c. Core Subassembly Dismantler. The Core Subassembly Dismantler (see Progress Report for October 1963, ANL-6801, p. 19) has been used to disassemble two fuel subassemblies which have been removed from the reactor. Both had been in the primary tank sodium, but were not irradiated.

The dismantler has now been equipped with the adaptors and fixtures necessary to permit disassembly of the other six subassembly configurations used in EBR-II. Trial operations on the blanket, safety, and control subassemblies will be carried out as soon as they become available.

An additional muffler reduced the noise level of the dismantler cooling system to a satisfactory level. A pump bypass circuit has also been added to the cooling system which will permit operating the system at the air flow required for cooling rather than at a fixed maximum flow, consequently extending the life of the high-efficiency filters. A minor modification is being made to permit the tie bolt nut holding the blanket section to be unscrewed rather than to shear the bolt as originally planned.

d. Fuel Element Decanner. The Fuel Element Decanner in the Argon Cell has decanned approximately 800 unirradiated sodium-bonded fuel elements during the past six months as part of the shake-down tests. The sodium was found to be more adherent at room temperature in the high-purity Argon Cell atmosphere than in previous dry box tests with a less pure

atmosphere. This additional adherence of the sodium caused some problems with the proper movement of scrap through the machine. The scrap problem was solved by heating the chopper unit and by a small increase in the gear-tooth spacing in the chopper which crimps and tears the scrap into short lengths.

Some intermittent stoppage has occurred in the flow of fuel through the decanner. This could have resulted from either slippage in the decanner drive mechanism, or from jamming of the entrance to the chopper by a mixture of tacky sodium and small fuel chips produced by the chopper. There was also some loss of these fuel chips from the chopper entrance.

The decanner slippage has been corrected; also the drive chain mechanism is being changed to increase its reliability. The flow of fuel into the chopper is expected to be aided and the loss of chips reduced by a new guide-tube design that is ready for testing. This tube encloses the fuel as it leaves the decanner until it is inside the chopper. The tube can be heated if it is found necessary to reduce the resistance of the sodium to the passage of the fuel.

During the decanning of the 800 fuel elements, the decanner tool broke more frequently than normal. Investigations revealed that the breakage was principally due to improper heat treatment of the tool blank material as obtained from the manufacturer. New tools will be prepared as soon as certified blanks of the original material (REX AA) can be obtained. In the meantime, a more ductile tool steel (M2) is being used.

e. Fuel-preparation Tests. The initial injection casting runs with uranium-fissium fuel were undertaken in the Argon Cell. Four casting runs were made; the first two have been processed through the demolding and pin processing station. Results are shown in Table XI.

Table XI. Fuel Cycle Production Data

Cast Run No.	Charge (kg)	Cast Metal (kg)	Total No. Castings	No. Acceptable	No. Rejected
.21	10.1	8.06	100	86	14
.22	11.6	8.42	90	63	27
.23	11.2	8.19	Processing Incomplete		
.24	9.47	6.48	Processing Incomplete		

The first series of test runs on the bonding equipment has been completed with the electrical cyclic bonder and a pneumatic bonder. Analysis of the early portion of the tests (electrical cyclic bonder) indicated that, while the annular bond appeared satisfactory, nearly all of the elements showed a large void either just above the fuel or just below the

restrainer. Increased time of bonding did not correct this condition. High-speed photographs of the action of the cyclic bonder indicated that the machine was not imparting enough energy to the fuel element. While possible modifications to this bonder were being considered, an alternate machine, pneumatically actuated, was put into operation. The results from this machine were encouraging. Data from this initial series is presented in Table XII.

Table XII. Results of Two Types of Bonding Runs

Run No.	No. of Pins	Bonder Type*	Time (min)/ Temp. (°C)	Impacts	Results		Reject for Voids**		
					Accept	Reject	Ann.	Bubble	Trap
1	17	E	30/500	3500	0	17	x	x	x
2	17	E	60/500	7000	0	17	x	x	x
3	17	E	120/500	14000	0	17	x	x	x
4	39	E	60/500	7000	0	39	x	x	
5	39	E	120/500	14000	0	39		x	
6	39	E	360/500	42000	0	39		x	
7†	20	E	240/500	28000	0	20		x	
8	3	P	1/500	100	3	-			
9	3	P	3/500	300	3	-			
10	3	P	4/500	400	3	-			
11	3	P	5/500	500	3	-			
12	3	P	7/500	700	3	-			
13	3	P	8/500	800	3	-			
14	3	P	10/500	1000	3	-			
15	5	P	Incl. ampl. variation at 500°C						
16	5	P	"	100	Not evaluated				
17	11	P	"	300	"				
18	6	P	"	500	"				
19	14	P	"	700	"				
				1000	"				

*E = electrical cyclic; P = pneumatic

**Annular void = void greater than 1/16 x 3/32-in. in annulus;
Bubble = void above pin or below restrainer greater than 1/16 x 1/16 in.;

†Trap = Sodium of tube wall above normal level
These rods were removed and directionally cooled (bottom to top).

G. FARET

1. General

During the month the principal Laboratory effort has been related to refinement of cell and equipment arrangements, and to conversion of these details into firm layout requirements for the architect-engineer. Particular emphasis has been placed on the evaluation of requirements for layout of vault equipment.

The initial submittal from Bechtel of the construction Package I specifications and drawings has been received at the Laboratory. The submittal is complete except for the excavation drawings which will follow shortly on a schedule which is not expected to delay the completion date for the entire package.

United Engineers and Constructors, Inc. has been selected as the general contractor. Initial orientation and information meetings have been held for the benefit of contractor personnel.

2. Safety Analysis

The Laboratory review of the Preliminary Safety Analysis Report has been completed. Final editing is in progress.

3. Facility Design

a. Cell Atmosphere. The FARET cell is a shielded, leak-resistant, containment structure, 20 ft wide by 60 ft long by 35 ft high, with a volume of 42,000 cu ft. This structure surrounds the reactor and the wet fuel-storage tank, and houses the remotely operated fuel-handling and disassembly machinery. Normally the cell will contain an argon atmosphere, but occasionally it may be necessary to change the atmosphere from argon to air.

Two techniques for changing the cell atmosphere have been considered: evacuation and displacement. Design considerations associated with the evacuation technique has made the displacement method appear to be the more practical.

In order to determine the feasibility of the displacement method, the amount of mixing that may take place between the gases during the displacement process must be known. An experimental facility (see Figure 7), comprising a sealed tank 4.5 ft in diameter and 12.5 ft in height, with windows and gas-detection probes at various elevations, was constructed. An inlet distribution pipe for argon is located near the bottom, and a 4-in.-diameter outlet at the top is connected to a blower. The gas-detection probes were connected to a 0 to 5 percent oxygen analyzer through a group of selection valves. Lights, heater, and sheet metal pieces (vertical obstructions) simulating cell equipment were located inside the tank.

Argon was admitted to the air-filled tank at a predetermined rate of flow for a given period of time. This established (a) the calculated rate of vertical movement of a theoretical interface between the argon and air in the tank, and (b) the total volume of argon in the tank. When the theoretical interface approached the vicinity of a given detection probe, the probe was opened and the gas in the vicinity of the probe was analyzed. In

this manner the amount of mixing and diffusion at the interface could be crudely determined. After each run, oxygen content was determined at all five probe points, and the amount of air remaining in the tank was estimated.

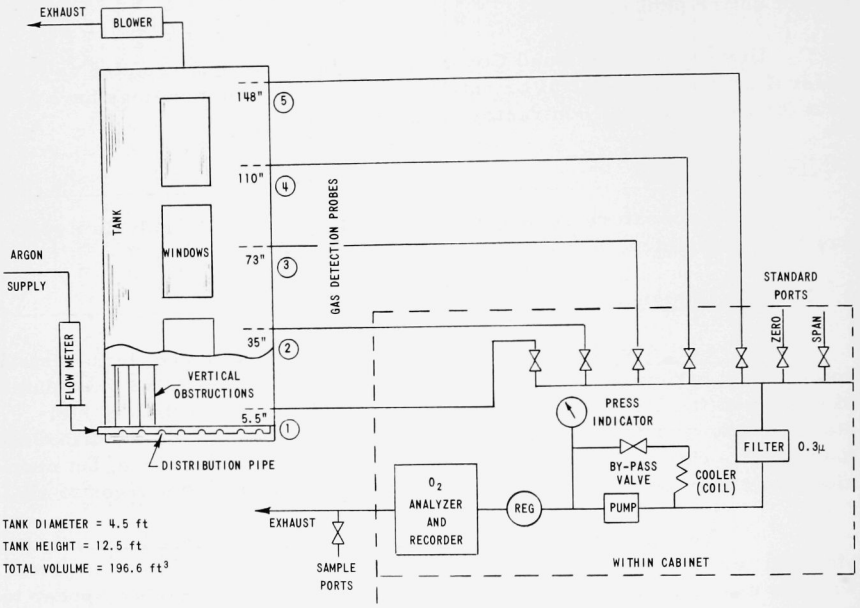

Figure 7. System for Gas Diffusion Study

Some runs were made also with a smoke-filled tank and the existence and condition of the interface visually noted.

The movement of the interface was studied by two experimental techniques. First, the theoretical interface was moved at a constant velocity through the range from 4 to 20 ft/hr for the total height of the tank. Secondly, the interface velocity was varied through the range from 12 to 20 ft/hr for the first 3 ft of tank height. Then for the remaining $9\frac{1}{2}$ ft, the velocity was held constant at 40 ft/hr. The latter method insured that the gas was not turbulent upon entering the tank and served to establish a section of still gas that would act as a plenum chamber or buffer region for the incoming gas when the flow rate was increased.

The results of fourteen runs are given in Table XIII. The oxygen percentages are from readings taken immediately after the run. The Comments column notes the various conditions, i.e., blower on, lights and heater on, vertical obstructions, and extent of overfill or underfill during the run.

Table XIII. FARET Cell Gas Diffusion Study

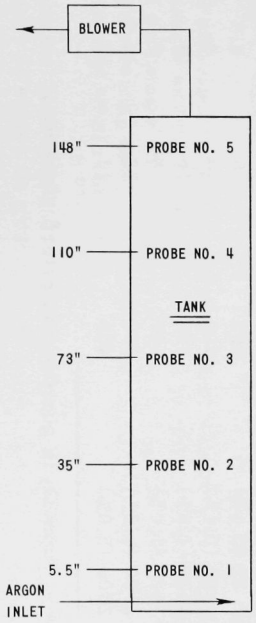

GAS INTERFACE MOVEMENT ft/hr	OXYGEN ANALYZER READING, v/o					COMMENT
	PROBE NO. 1	PROBE NO. 2	PROBE NO. 3	PROBE NO. 4	PROBE NO. 5	
CONSTANT VELOCITY						
4	0	0.07	1.25	>5	>5	4% OVER FILL
6	0	0	0.06	4.12	>5	4% OVER FILL
8	0	0	0	4.42	>5	
12	0	0	0	0.24	>5	NO. 5 RECORDER 3.4 AFTER 12% OVER FILL
16	0	0	0.05	0.10	2.75	8% OVER FILL
20	0	0	0.05	0.10	2.6	8% OVER FILL
VARIABLE VELOCITY						
12 - 40	0.3	0.35	0.39	0.58	2.89	FIRST 3 ft. OF TANK AT 12 ft/hr
12 - 40	0.26	0.27	0.27	0.51	2.75	BLOWER ON, ΔP = 0.32" WG
16 - 40	0.16	0.21	0.28	0.35	1.75	BLOWER ON, 5% OVER FILL
20 - 40	0.34	0.37	0.42	0.79	>5	BLOWER ON, 10% UNDER FILL
16 - 40	0.38	0.39	0.39	0.39	0.39	BLOWER ON, LIGHTS & HEATER ON, VERT OBS.
20 - 40	0.36	0.38	0.38	0.38	0.38	BLOWER ON, LIGHTS & HEATER ON, VERT OBS.
20 - 40	0.46	0.47	0.47	0.47	0.47	BLOWER ON, LIGHTS & HEATER ON, VERT OBS.
20- 41.6	0.70	0.70	0.70	0.70	0.70	BLOWER ON, LIGHTS & HEATER ON, VERT OBS.

Additional runs checked the importance of establishing the still section of gas in the tank before increasing the flow. The tank was filled at a flow equal to an interface movement of 40 ft/hr and timed for one complete volume. The gas mixed badly and there was no indication of an interface. A duplicate run with a smoke-filled tank verified the lack of an interface.

It is concluded that by controlling flow and distribution of the gas, a relatively small amount of diffusion and mixing between gases takes place and a fairly distinct interface exists. Furthermore, the existence of a still gas area facilitates the filling of a given volume in a shorter period of time, allows a very rapid interface movement, and reduces the fill time which, in turn, reduces diffusion and provides a more effective gas-changing process.

The test data indicate that after a changeover, the oxygen concentration in the cell due to the remaining air may be of the order of a few percent depending on the overfill of argon allowed during the transfer. Further purification of the cell atmosphere from this level to some point below 100 ppm oxygen would be achieved by circulation of the gas through a purification system.

An analysis of the dynamic behavior of a hydrogen-catalytic purification system was made to determine the approximate time required to achieve oxygen levels below 100 ppm in the cell. In this study, the air inleakage rate into the cell was taken to be 14 ft^3/day. Two purification-circulation rates were considered, 200 ft^3/min and 400 ft^3/min, and for each of these rates 40, 20, and 10 ppm oxygen was assumed present in the return gas from the purification system. Complete and uniform mixing of the return gas with the cell gas was also assumed. The results of the analysis are summarized in Table XIV.

Table XIV. FARET Cell Atmosphere Purification Study

O_2 in Cell Initially, ft^3 (%)	Purification Rate, ft^3/min	Time to Attain 100 ppm O_2 Level, hr		
		10*	20*	40*
42 (0.1%)	200	8	8.5	9
42 (0.1%)	400	4	5	6
420 (1.0%)	200	16	18	20
420 (1.0%)	400	8	9	10
2100 (5.0%)	200	22	24.5	28
2100 (5.0%)	400	11	12	13

*ppm O_2 in purification return stream.

b. In-cell Equipment Transfer. A preliminary study was made to determine the feasibility of utilizing the fuel-transfer area for the transfer of equipment to or from the cell. Such a scheme appears to have merit.

The basic guide lines used in the study for equipment transfer are that (1) the cell containment criteria will be maintained, (2) purity of the argon atmosphere of the cell will be maintained, (3) the largest piece of equipment to be transferred will be the reactor vessel head, including the integral control rod drive mechanisms, (4) radioactive contamination will be present, and (5) sodium contamination will be present. The use of a lock between the cell and fuel transfer tunnel (see Figure 8) appears to satisfy these requirements. The lock, 8 ft 6 in. in diameter by 5 ft deep, is comprised of a hinged internal cover and a bottom closure, the latter being made by a hydraulic hoist platform. For equipment which exceeds the depth of the lock, metal extensions to the bottom side of the cell would be used as a temporary part of the lock. The lock would be charged with argon so that equipment transfer may be made without contaminating the argon atmosphere in the cell.

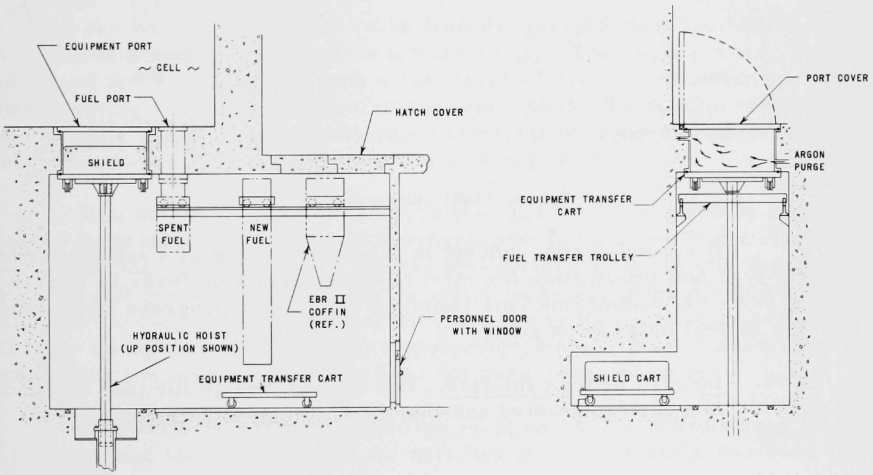

Figure 8. Preliminary Scheme of Equipment Transfer for FARET Cell

The atmosphere in the transfer tunnel will be air. Decontamination, maintenance, and other functions can be performed in this area. The transfer of equipment out of the transfer tunnel to the building floor would be through a ceiling hatch. A trolley cart arrangement would be used to transfer equipment within the tunnel.

Spent fuel will be transferred from the fuel port to and through the hatch by means of either an EBR-II-type interbuilding transfer coffin or an off-site transport coffin. New fuel will be introduced through the fuel port using a new fuel transfer container.

4. Component Development

a. Cell Penetrations. A design (see Figure 9) for a sealed, straight-through cell penetration has been completed. This design incorporates the use of underwater or submarine-type electrical cable. It is planned to fabricate a mockup and to check out the feasibility of the design.

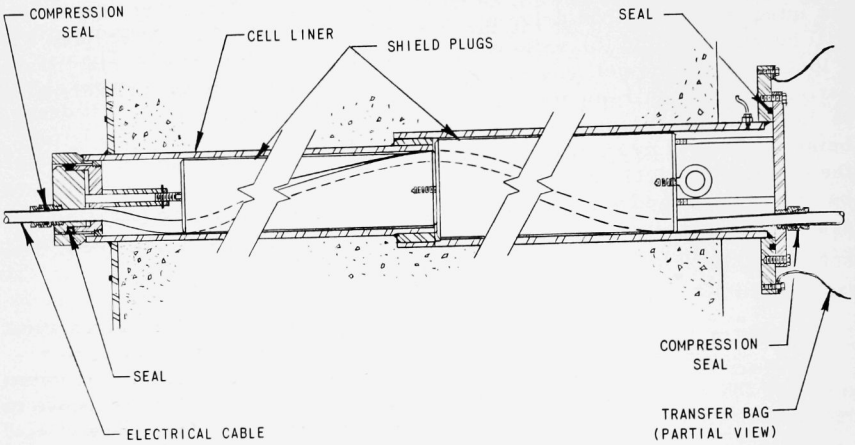

Figure 9. FARET Cell Penetration

A second design concept is based on the use of a sealed, curved, conduit-type cell penetration for in-core instrumentation leads by means of underwater or submarine type cable. A study is in progress to determine the type of seal plugs to be used.

b. In-core Instrumentation. The furnace design for test conditions up to 650°C has been completed and the major components ordered from the shops.

The specifications for the high-temperature (2800°C) furnace needed to develop sensors to determine fuel pin temperature have been prepared. The proposed test procedures will consist mainly of determining the performance characteristics and long-term stability of thermocouples. Other investigations, however, will include a study of the compatibility of sensor materials with fuels, the stability of the emf characteristics of thermocouples after temperature cycling, and an evaluation of material performance at these very high temperatures.

5. Fuel Assembly Sodium Flow Test Facility

A draft report of proposed procedures to install and operate a test loop for FARET fuel assemblies has been prepared. A major cause of concern has been the trouble encountered in resolving the results of pipe stress calculations.

This system is not unlike many other sodium loops that have been built. The arrangement of the facility in the deep pit of D-308 coupled with an operating procedure which excludes people from the pit while the pump is running provides adequate protection to people even in the unlikely event of a complete break of a sodium pipe under pressure.

6. CP-5 In-pile Experiment

The vacuum system for the FARET In-pile Gas Gap Experiment (heat transfer in the fuel element) has been simulated and the vacuum control system installed for checkout.

The variable leak rate valve (see Progress Report for March 1964, ANL-6880, p. 47) did not operate satisfactorily. The copper tubing work-hardened and cracked after only a few hours of service. Second, the valve, representing a very high resistive element, caused the system response to be too slow. To improve the system performance, a needle valve was selected as the new control element and is being studied.

The thermocouples to measure the clad temperature have been received from the vendor. These thermocouples have a preformed tip of the so-called "Cut Spade" type. This design provides a strong attachment to the clad and gives the least error between the actual and indicated temperature of the clad surface. The original tip dimensions had to be modified slightly so that the vendor could manufacture them. The thermocouples for measuring the fuel temperature have not been received as yet.

The assembly and wiring of the instrument console has been started. All equipment for this phase of the instrument requirements has been received.

III. GENERAL REACTOR TECHNOLOGY

A. Experimental Reactor and Nuclear Physics

1. High-conversion Critical Experiment

The core now loaded in the High Conversion Critical Experimental Facility (ZPR-VII) has an atom ratio of 1.33 ($H:U^{238}$) and a volume ratio of 0.44 (H_2O/UO_2). It is fueled with 3 w/o enriched UO_2, as 0.94-cm-diameter pellets, loaded into either 1.06-cm-diameter stainless steel or aluminum tubing. The fuel rods are spaced in a grid having a 1.17-cm triangular pitch. The current core has a height of 122 cm and has a central stainless steel-clad fueled zone, approximately 25 cm in diameter, surrounded by an aluminum-clad fueled annulus. Some corrected measurements for a number of micro-parameters made with this core are shown in Table XV.

Table XV. Micro-parameter Measurements Made with the 25-cm Stainless Steel-clad Central Fuel Zone Surrounded by an Aluminum-clad Annulus Fueled Zone

Measurement	Value
Fission cadmium ratio of U^{235}-C_{25}	
Measured in fuel element	2.6^- ± 0.1*
Measured in moderator	2.7 ± 0.1
Ratio of epi-to-subcadmium fissions, ρ_f^{25}	0.64^+ ± 0.03*
Ratio of bare U^{235} foil fissions (moderator/fuel)	1.05^+ ± 0.004*
Thermal disadvantage factor	1.10 ± 0.03
Capture cadmium ratio of U^{238} (C_{28}) (by dysprosium substitution)	1.10 ± 0.001
Ratio of epi-to-subcadmium captures, ρ_c^{28}	9.99 ± 0.06

* The superscript sign indicates the value cited is either slightly less (-) or slightly higher (+) than shown.

After the balance of the measurements with this core are completed, temperature coefficients of an all aluminum-clad core will be determined. Then a number of two-zone systems in which the central zone will be very densely packed will be studied, and an attempt to achieve zero or negative buckling will be made. For the densest loading reported, with an atomic ratio in the fuel zone of 1:1 H/U^{238}, the buckling is small. It is not known, however, at what loading density the buckling will be zero. The experiments will provide data which can be used to resolve the differences between experimental results and theoretical predictions in this region of interest.

B. Theoretical Reactor Physics

1. Orthonormal Expansion of Neutron Spectra

The error sensitivity of the orthonormal expansion methods used in the activation cross sections has been explored. Quantitative estimates of propagation of error in the Gram-Schmidt method and least-squares method for the chosen test problem[3-5] has been obtained by introducing a random number game. In this game, one modifies the cross sections $\sigma_i(\epsilon)$ according to the rule

$$\sigma_i(\epsilon)' = \sigma_i(\epsilon)(1 + \delta_i); \quad i = 1, 2 \ldots n, \tag{1a}$$

where δ_i can assume only three values:

$$\delta_i = \begin{cases} \Delta \\ 0, \\ -\Delta \end{cases} \tag{1b}$$

with Δ a positive constant representative of magnitude of the experimental error.

Using the modified set of cross sections $\{\sigma_i'\}$, the original computations are repeated, and the relative error

$$E_n(\Delta) = \int_0^\infty |H_n(\epsilon) - \phi(\epsilon)| d\epsilon \tag{2}$$

is determined. If a sufficient number of trials of this random number game are executed, one can obtain estimates of the error which is propagated to the approximations $H_n(\epsilon)$, that is, for each trial one determines $E_n(\Delta)$. For N such trials, one can find the mean value of the sample, $\bar{E}_n$, as well as the standard deviation, S_n, of the sample. Thus, if $(E_n)_i$ is the value of E_n for the ith trial, then

$$\bar{E}_n = \frac{1}{N} \sum_{i=1}^{N} (E_n)_i; \tag{3a}$$

$$S_n = \left[\frac{1}{N} \sum_{i=1}^{N} \left((E_n)_i - \bar{E}_n \right)^2 \right]^{1/2}. \tag{3b}$$

---

[3] Reactor Development Program Progress Report for October 1963, ANL-6801, p. 41.
[4] Reactor Development Program Progress Report for December 1963, ANL-6810, p. 27.
[5] Reactor Development Program Progress Report for January 1964, ANL-6840, p. 53.

The mean $\overline{E}_n$ and standard deviation S_n have been determined for both the Gram-Schmidt and least-squares methods in the range $0.10 \geq \Delta \geq 0.001$, which corresponds to an experimental error range between ten percent and one-tenth of a percent for the cross sections utilized in these computations.[4] The results of the random number game are presented in Tables XVI and XVII for the Gram-Schmidt and least-squares method, respectively. For each method the sequence of cross sections yielding the best fit of the fission spectrum was determined before employing the random number game. The sensitivity of these methods to cross-section error is apparent.

Table XVI. $\overline{E}_n$ and S_n for the Gram-Schmidt Method

	$\Delta = 0.10$		$\Delta = 0.05$		$\Delta = 0.01$		$\Delta = 0.005$		$\Delta = 0.001$	
n	$\overline{E}_n$	S_n	$\overline{E}_n$	S_n	$\overline{E}_n$	S_n	$\overline{E}_n$	S_n	$\overline{E}_n$	S_n
5	0.5837	0.1245	0.4830	0.0597	0.4582	0.0146	0.4550	0.00663	0.4550	0.00130
6	0.5595	0.0921	0.4752	0.0494	0.4451	0.0105	0.4447	0.00517	0.4440	0.000990
7	0.5494	0.0940	0.4299	0.0329	0.3994	0.00751	0.3980	0.00330	0.3978	0.000678
8	0.7428	0.285	0.4892	0.151	0.3258	0.0218	0.3199	0.0106	0.3168	0.00210
9	1.017	0.393	0.5867	0.199	0.3398	0.0365	0.3200	0.0164	0.3127	0.00348
10	0.921	0.464	0.5258	0.191	0.2455	0.0314	0.2241	0.0146	0.2159	0.00217

Table XVII. $\overline{E}_n$ and S_n for the Least-squares Method

	$\Delta = 0.10$		$\Delta = 0.05$		$\Delta = 0.02$		$\Delta = 0.01$		$\Delta = 0.005$		$\Delta = 0.001$	
n	$\overline{E}_n$	S_n	$\overline{E}_n$	S_n	$\overline{E}_n$	S_n	$\overline{E}_n$	S_n	$\overline{E}_n$	S_n	$\overline{E}_n$	S_n
4	0.278	0.0762	0.2011	0.0378	0.1664	0.0104	0.162	0.00496	0.1605	0.00223	0.1604	0.000483
5	1.807	1.285	0.9160	0.6333	0.393	0.238	0.233	0.105	0.1661	0.0439	0.1387	0.00774
6	4.115	2.610	2.066	1.305	0.844	0.520	0.444	0.258	0.250	0.1287	0.1083	0.0267
7	3.855	2.654	1.933	1.325	0.783	0.527	0.404	0.259	0.219	0.125	0.0829	0.0186
8	4.047	2.860	2.026	1.430	0.818	0.572	0.420	0.285	0.226	0.142	0.0824	0.0299

2. Computation of New 22-group Constants for Fast Reactor Calculations

An interim set of 22-group constants for fast reactor calculations has been prepared based on recent microscopic cross-section data. Although not yet in the final stage of refinement, the constants have been used for a variety of fast reactor calculations, including existing critical experiments as well as large conceptual systems capable of up to ~1000 MWe output.

In addition, the constants also permit inelastic scattering to sixteen groups of lower energy. Twelve groups have actually been used in preliminary analyses. Six to eight groups were frequently used to describe inelastic scattering in previous compilations. The basic group structure was chosen to afford a neutron energy distribution applicable to the problems of current interest, including those systems with capability of ~1000 MWe. The lower energy boundary of the lowest energy group is 30 eV.

Preliminary analyses made with these constants show that predicted criticality is not very much different from predictions with previously published multigroup compilations. However, spectral predictions and related reactivity effects are somewhat different from predictions based on previous compilations.[6,7] In particular, predicted fission cross section ratios and prompt neutron lifetime appear to be in better agreement with experimental results. The number of predicted fission and capture events below 9 keV appear to be larger than previously predicted. The latter "spectral index" is quite significant in predicting the Doppler coefficient of reactivity in many systems of interest.

3. Calculated ZPR-III Prompt-neutron Lifetime by 1/v Material Insertion

Multigroup analyses of prompt-neutron lifetime of ZPR-III fast critical assemblies have been often calculated by simulating the insertion of a small amount of 1/v absorber throughout the core and reflector regions. Generally, this fictional 1/v absorber is assumed to augment only the absorption properties of the regions and not the transport properties. The fractional change in lifetime, if the transport cross section is also simultaneously augmented, has been calculated for a few ZPR-III assemblies: Nos. 14, 22, 23, and 32, which represent U^{235}-fueled systems with graphite, U^{238}, aluminum and stainless steel diluents, respectively. In all cases a 30-cm-thick, high-density, U^{238}-containing reflector was used. The resultant ratios of lifetimes by 1/v augmentation of both transport and absorption cross sections relative to only 1/v absorption augmentations are: 0.988, 0.991, 0.984, and 0.984, respectively, for the four assemblies.

4. Relative Calculations of Prompt-neutron Lifetimes for Reflected and Bare ZPR-III Core Compositions

The effect of the 30-cm-thick, high-density reflector upon the prompt-neutron lifetime, ℓ_p, of a corresponding bare system has been calculated by the 1/v insertion method for the previously described ZPR-III case Nos. 14, 22, 23, and 32. The relative ratios of ℓ_p for the reflected to the bare systems are: 1.04, 1.10, 1.22, and 1.15, respectively, for these systems.

5. ZPR-VII Data Analysis

New versions of U^{235} and U^{238} cross sections, on library tape supplied by Hanford, have been added to the GAM-I-library. These cross sections differ from the old GAM-I versions in the values of σ_c, σ_f, and $\nu\sigma_f$, and in the U^{238} resonance parameters. The use of the new U^{235} and U^{238} tapes in the case of the Hi-C square 1.24-cm Al-clad lattice reduced reactivity by about

[6] S. Yiftah, D. Okrent, and P. A. Moldauer, Fast Reactor Cross Sections - A Study Leading to a Sixteen-Group Set, Pergamon Press, New York (1960).

[7] G. E. Hanson and W. H. Roach, Six and Sixteen Group Cross Sections for Fast and Intermediate Critical Assemblies, LAMS-2543 (1961).

3% from the case where the original values were used. The use of the new version reduces much of the discrepancy which exists between theory and experiment (see the Reactor Development Program Progress Report, ANL-6808 and ANL-6810, November and December 1963, respectively).

6. Total Neutron Cross Sections

A Fortran code is being written to determine Breit-Wigner single-level resonance parameters from experimental data on total cross sections at various energies. Initial guesses are made on the value of resonance parameters and a least-squares fit is made to improve on the initial values. Cross-section contributions from potential scattering and the tails of resonances outside the energy range under consideration are kept constant throughout the calculations. Angular momenta $\ell = 0$, 1, and 2 are allowed. Since the code is designed to fit data in the keV region as determined from measurements made with the Van de Graaff facility, Doppler effects for the resonances under study are quite negligible and resolution effects are small.

Test problems have been run for which the "experimental" cross sections were computed by a preliminary Fortran code. The calculated resonance parameters converged rapidly to the correct values for these problems. At present the code is being modified to include estimates of the errors in the derived resonance parameters, which are of considerable interest when actual experimental cross sections are being fit.

7. Numerical Analysis

One of the most convenient methods of representing mathematical functions for use in digital computers is by storing the coefficients of their expansion in Chebyshev polynomials. This representation is numerically stable and may be used to approximate the function to any desired accuracy up to the maximum available.

For approximating the natural logarithm over the range $1/\sqrt{R} \le x \le \sqrt{R}$, an expansion of the form

$$\ln x = \frac{x - 1}{x + 1} \sum_{k=0}^{N} c_{2k}\, T_{2k}(y),$$

where $y = (x - 1)/s(x + 1)$ and s is selected so that $y(\sqrt{R}) = 1$, has been found to be more efficient than other popular expansions. For $R = 2$ and $N = 12$, the maximum relative error is less than 0.5×10^{-28}; for $R = 10$, and $N = 24$ the same accuracy is obtained. Tables of the coefficients for these two values of R accurate to 28 decimal places have been computed on the IBM-1620 computer.

C. High-temperature Materials Development

1. Resistance to Corrosion by Lithium

Molybdenum, tantalum, niobium, and tungsten, as well as their alloys, are generally considered as potential containment materials for high-temperature lithium. However, little information is available pertinent to corrosion and solubility of these materials above 1000°C. Accordingly a program is being conducted to gain basic knowledge of the behavior of these materials on exposure to the liquid and vapor phases of lithium.

High-temperature, liquid-metal testing techniques have been developed, and capsules for the study of the corrosion and solubility of molybdenum, tantalum, and niobium have been prepared from high-purity arc-melted rod stock. They are loaded with lithium in an inert atmosphere and are vacuum-sealed by electron-beam welding.

One of the molybdenum capsules containing lithium has been tested for 100 hr in a vacuum (10^{-6} torr) furnace at 1000°C. No lithium leakage developed during the test period, but there was a slight, nonuniform discoloration of the external surface of the capsule. This capsule is now being prepared for chemical and metallographic analyses. Similar tests are being conducted with capsules of other materials.

2. Thorium and Thorium-base Fuels

a. Properties. In the core-blanket region of a reactor in which thorium-232 is used, a chain of nuclear reactions takes place in which neutron irradiation first converts thorium-232 to thorium-231 by an (n, 2n) mechanism, and the thorium-231 decays by beta emission to protactinium-231; neutron adsorption converts the protactinium-231 to protactinium-232, and this decays by beta-emission to uranium-232; further neutron absorption converts the uranium-232 to highly fissile uranium-233. A valuable nuclear fuel is thus produced from thorium, which is relatively abundant; but the complicated chain of reactions leads to intermediate products and to many byproducts that complicate the properties and reactor behavior of both the thorium and the uranium.

In addition, some of the values of properties reported for thorium were obtained with samples that were produced before large-scale thorium-refining techniques were sufficiently advanced, and many alloys of thorium have never been thoroughly investigated. Work is therefore under way to study the physical and mechanical properties of thorium and its alloys, as well as the fabricating characteristics and reactor behavior of these materials.

Chemical analyses of the best grades of thorium available in this country have been completed and their lattice parameters measured. Crystal-bar thorium supplied by Metal Hydrides, Inc. is low in hydrogen, carbon, and nitrogen, but high in oxygen and iron (see Table XVIII). Electron-beam-melted thorium, represented by a button made specially for this investigation by the Ames Laboratory through the courtesy of F. H. Spedding and D. T. Peterson, is very low in oxygen, but high in nitrogen, tantalum, and tungsten. This circumstance enabled us to determine the effect of oxygen on the lattice parameter of heat-treated specimens. The lattice parameter of thorium increases with impurity content, temperature and duration of heat treatment, and subsequent cooling conditions. Specifically, the lattice parameter increases with the interstitially dissolved impurity content. That part of the lattice-parameter increase, however, that is due to the oxygen contamination can be reversed by taking the oxygen out of solution with a subsequent heat treatment (see Tables XIX and XX). The low-oxygen Ames thorium, which did not show this reversibility, had the same lattice parameter after various heat treatments (see Table XXI).

Table XVIII. Composition of High-purity Thorium

		Metallic Impurities*								Interstitial Impurities			
No.	Material	Al	Cu	Fe	Nb	Si	Ta	W	Zr	H	C	N	O
B794	Crystal Bar									2	7	5	45
	Lab. I	<20	4	80	nd	8	nd	nd	nd				
	Lab. II	7	<5	30	nd	10	nd	nd	10				
	Crystal Bar, Arc-melted												
B772	Initial Conditions	15	5	15	nd	16	nd	nd	5	14	27	(30)	39
B828	Improved Conditions									1	7	4	88
B839	Ames Thorium, Electron-beam Melted	<4	<5	10	20	7	200	210	1	0.3	2	130 to 175	6

nd - not detected; *all other elements below limits of spectrochemical detection.

Table XIX. Effect of Heat Treatment on Lattice Parameter of Crystal-bar Thorium

No.	Heat Treatment			Lattice Parameter, a_0, Å
	Temperature, °C	Time, hr	Cooling	
1	As Received			5.0840
2	700	2	Furnace Cooled	5.0842
3	700	2	Oil Quenched	5.0848
4	900	2	Furnace Cooled	5.0855
5	900	2	Oil Quenched	5.0857
5	Subsequently 900	2	Furnace Cooled	5.0851

Table XX. Effect of Heat Treatment on Lattice Parameter of Arc-melted Crystal-bar Thorium

No.	Heat Treatment			Lattice Parameter, a_0, Å
	Temperature, °C	Time	Cooling	
1	700	2 hr	Furnace Cooled	5.0865
2	700	2 hr	Oil Quenched	5.0887
3	700	3 wk	Water Quenched	5.0897
3	Subsequently 700	2 hr	Furnace Cooled	5.0871

Table XXI. Effect of Heat Treatment on Lattice Parameter of High-purity Ames Thorium

No.	Heat Treatment			Lattice Parameter, a_0, Å
	Temperature, °C	Time, hr	Cooling	
1	500	0.5	Furnace Cooled	5.0857
2	900	2	Furnace Cooled	5.0863
3	900	2	Water Quenched	5.0861

The room-temperature lattice parameter of the highest-purity thorium is 5.0840 ± 0.0001 Å. Its theoretical density is 11.728 g/cm^3, in agreement with the best literature values.

The data suggest strongly that genuinely high-purity thorium may be prepared by a combination of the iodide-decomposition process (Metal Hydrides) with subsequent electron-beam melting (Ames process).

3. Irradiation of Thorium-base Fuels

An instrumented capsule, designed to evaluate the irradiation behavior of refractory-alloy-clad thorium-uranium and thorium-uranium-plutonium fuel alloys, has been inserted in a vertical thimble in the CP-5 reactor. Temperature control of the specimens is attained by flowing a gas of variable composition through a 0.13-mm-thick annulus between the specimen container and the outer seal tube. Helium and nitrogen can be selectively used or proportionately mixed to provide the desired thermal conductivity of the annulus which, in turn, controls the specimen temperatures. This method of temperature control has been successful in the MTR reactor for irradiation of full-length EBR-II fuel pins.

Some of the MTR capsules were observed to be susceptible to temperature fluctuations as a function of the helium flow rate. The CP-5 capsule does not show this characteristic. However, by varying the ratio of helium to nitrogen, temperature control of the specimens can be maintained over a range of 300°C.

The fuel specimens, all clad in Nb-1 w/o Zr tubing, are 50 mm in length and 3.66 mm in diameter. The fuel alloys are Th-35 w/o Pu, Th-20 w/o U-20 w/o Pu, and Th-20 w/o U. The claddings have a wall thickness dimension of 0.38 mm and an inside diameter of either 3.96 mm or 6.52 mm. The pins are NaK bonded to the clad but otherwise unrestrained.

The specimens are installed in the capsule in tandem, that is, one is placed directly above the other. In order to balance the heat generation of the capsule to the flux profile within the fuel tube, specimens having the highest concentration of fissile material were placed at the extreme ends of the specimen chamber.

The maximum specimen temperature is being maintained at 740°C. The maximum cladding temperature is 550°C.

4. Dissolution Kinetics in Liquid Metals

The dissolution kinetics of Type 304 stainless steel (SS) in 58 w/o bismuth-42 w/o tin eutectic alloy are under investigation to evaluate the potential corrosion problem of 304 SS in the EBR-II rotating seal by the low-melting eutectic alloy. The present work has also been useful in establishing experimental techniques to be used in determining the dissolution kinetics of refractory metals in a number of liquid metals.

The experimental method consists of immersing a 304 SS disc, 6.08 cm in diameter and 0.294 cm thick, in 500 cm^3 of Bi-Sn eutectic alloy. The disc is rotated at a constant angular velocity and the liquid is sampled at temperature as a function of time. The Bi-Sn samples are analyzed for iron, chromium, nickel, and manganese by the spectrographic method together with specially prepared standards. In addition to the solution-rate data, material solubility data for the Fe, Cr, Ni, and Mn in the eutectic alloy have been obtained for times up to 100 hr at temperatures of 860, 650, and 450°C.

The rotation speed of the disc has been reduced from 100 rpm to 10 rpm at temperatures of 860 and 650°C to determine the effect of velocity on the dissolution process. The Bi-Sn samples obtained at the lower rotational speeds are being analyzed at the present time.

Dissolution data obtained under the well-defined hydrodynamic flow conditions produced by the geometry of the rotating-disc sample can be compared with calculated liquid-diffusion-controlled dissolution rates (for rotating discs) to give insight into the dissolution mechanism. The results and a detailed discussion of the hydrodynamics of the system will be presented after the data from the latest dissolution runs are analyzed.

5. Elastic Moduli of High-temperature Materials

To measure the temperature dependence of the elastic moduli of materials which show promise in high-temperature reactor applications, a vacuum furnace has been constructed in which solid bar-shaped samples will be mounted. Pulsed ultrasonic waves will be propagated along the length of these samples, and the transit times of pulses passing a heated, indexed region in each bar will be measured. The indexing is done by machining one end to a smaller diameter than the rest of the bar.

The velocity of sound in the indexed region can then be calculated by knowing the length of this region and the transit time. Both shear wave velocities (V_S) and longitudinal velocities (V_L) are determined. Poisson's ratio can be calculated by means of the formula

$$\sigma = \frac{\frac{1}{2}(V_L/V_S)^2 - 1}{(V_L/V_S)^2 - 1}.$$

Young's modulus can be calculated from

$$E = \frac{V_L^2 \rho (1 + \sigma)(1 - 2\sigma)}{1 - \sigma},$$

where ρ is the density of the material.

A stainless steel rod, mounted in the vacuum furnace, was heated from room temperature to 800°C. A quartz transducer was mounted on the cool end of the rod, and ultrasound oscillating at 5 Mc/sec was propagated into it. The appropriate echoes could be followed and identified throughout the heating. The purpose of this test was not to measure transit times, but only to see how the sound pattern would behave as the sample was heated.

The main concern at this time is the reduction of the temperature gradient in the specimen. With the sample immersed into the furnace as far as it would go (i.e., as much of the bar heated as possible), observations were made of the temperature differences, which ranged from zero to a maximum of 15°C. In an attempt to reduce this gradient, the heating windings of the furnace are being rearranged.

In order to determine V_L and V_S, one could measure the transit times in the indexed region by two separate heating runs, one with a longitudinal wave-generating-transducer, the other with a shear transducer. A composite transducer, made of both longitudinal and shear transducers, might be used instead. A much more satisfactory way would be to measure the longitudinal

velocity and the delay time between the so-called trailing pulses, which are generated by virtue of the waveguide nature of the rod.[8] The delay between these pulses is a function of the shear wave velocity; the complete measurement could be done in one heating run with one transducer.

The velocity and delay time that must be measured are those pertaining to the small-diameter section of the rod. Unfortunately, the delay signals from the long length of large-diameter section obscure those from the short length of the thin section. It has been stated in the literature that threading the surface of the bar will cause the delayed pulses to be eliminated. Recent experience in this Laboratory indicates that simple threading of the rod does not in all cases eliminate the delayed pulses. Since this problem is of some importance to the study of modulus measurements at high temperatures, it will be the subject of further study.

A 2.5-cm-diameter bar of tungsten that had been pressed, sintered, and swaged supported sound waves very well, with a remarkably low attenuation. A 1.2-cm-diameter, 58-cm-long tungsten rod was also examined; echoes to 1125 μsec detected at 5 Mc/sec, corresponding to 580 cm of travel. The parameters of interest in the 2.5-cm-diameter tungsten rod were

Longitudinal wave velocity:	$(5.100 \pm 0.005) \times 10^5$ cm/sec
Shear wave velocity:	$(2.802 \pm 0.003) \times 10^5$ cm/sec
Poisson's ratio:	0.2838 ± 0.0008
Young's modulus:	$(3.87 \pm 0.03) \times 10^{12}$ dyne/cm^2.

D. Other Reactor Fuels and Materials Development

1. Zirconium Alloys

a. Corrosion in Superheated Steam

(i) Alloy Modification. Zirconium alloys that are corrosion resistant in superheated steam have been subject to surface embrittlement associated with oxygen absorption resulting from exposure to steam at 650°C. A reduction of the oxygen absorption-and-diffusion rate is being sought by immobilization of the metal structure through additional alloying components. In current tests alloys based on either crystal-bar zirconium or the Zr-1.1 w/o Cu-1.5 w/o Fe alloy were made that contained 9 to 22 w/o Be, 32 w/o Si, or 44 w/o Si. These alloys were homogenized by levitation melting and were then exposed to deoxygenated steam (static, refreshed conditions) at 650°C and 42.2 kg/cm^2 (600 psi) for periods of up to thirteen days.

---

[8] Peterson, R. G., Mechanical Vibrations in Solid Rods, ANL-6515, pp. 133-161.

Although none of the samples had satisfactory corrosion resistance, differences in behavior were great enough to indicate the possibility of achieving both the desired degree of microstructural stabilization and satisfactory resistance to corrosion. The best alloys were based on Zr-1.1 w/o Cu-1.5 w/o Fe and were relatively low in beryllium content. For example, the alloy containing 9 w/o Be had a dark, adherent corrosion product, was free of blister attack, and had a total weight gain of 27 mg/cm^2. Other alloys cracked or disintegrated into various numbers of pieces.

(ii) Electrical Measurements. An electrical study of thermally produced ions near surfaces in low-pressure gaseous environments at 500 to 750°C has continued (see Progress Report for March 1964, ANL-6880, p. 55). These ions have been previously related hypothetically with hydrogen-absorption phenomena in superheated-steam corrosion.

Platinum and stainless steel surfaces and precorroded zirconium alloy electrodes have been employed in recent tests. It is evident from the results that (1) free-ion effects are not limited to zirconium alloys; (2) modification of the environment by including air markedly increases the conductivity of the environment near surfaces, at a given low pressure; and (3) the volume leakage of the mica insulators employed in the hot zone of the test apparatus was appreciable but insufficient to account for the effects, which were reproduced qualitatively in the absence of hot-zone insulators.

2. Ferrous and Nickel Alloys

a. Corrosion in Superheated Steam. The 18 percent chromium, 8 percent nickel types of austenitic stainless steels do not resist corrosion by superheated steam as well as do some of the straight-chromium stainless steels (such as Type 406) or as well as do the higher-nickel alloys (such as Incoloy 800 or various Inconel alloys) including an aluminum-modified Incoloy. The effects on corrosion behavior of changing the temperature or pressure of the steam, or of modifying alloy composition, are not well known in all instances. The corrosion behavior in superheated steam of the relatively corrosion-resistant ferrous alloys is therefore being investigated in detail.

Refreshed static tests are being carried out at 750°C and 42 kg/cm^2 (30 ppm of oxygen). Defilmed-metal losses determined up to now are reported in Table XXII.

Incoloy 800 modified with various amounts of aluminum is being tested at 650°C and 42 kg/cm^2 in flowing (61-m/sec) steam containing 30 ppm of oxygen and 3.8 ppm of hydrogen. The samples have not been defilmed for the more recent inspections (56 days of exposure), but the weight gains for the material containing 3.8 w/o of aluminum suggest a corrosion rate that is very low.

Table XXII. Corrosion in Steam at 750°C and 42 kg/cm^2

Alloy	Metal Loss, mg/cm^2, after			
	7.0 days	14.0 days	21.0 days	28.0 days
Type 304	8.3	10.9	14.3	23.0
316	12.2			
321	12.9			
347	11.9			
406	0.4	0.2		
Inconel 600	9.4			
625	0.4	0.6		
X750	2.9	2.4		
Incoloy 800	6.7	7.2	6.8	6.8

In the March Progress Report (ANL-6880, p. 4) the belief was expressed that reduction of the oxygen content of the steam in BORAX-V through use of a catalytic recombiner could materially reduce the oxidation rate and susceptibility to stress-corrosion cracking of the austenitic stainless steel cladding. However, experimental work at Argonne and elsewhere demonstrates that a recombiner, regardless of any likely obtainable efficiency, would have no appreciable effect on the corrosion behavior of the austenitic stainless steel.

3. Nondestructive Testing

a. Ultrasonic Imaging. Motion-picture recordings made of the Kinescope during ultrasonic inspections of several flat fuel elements were recently completed. The films demonstrate the capability of the system for inspecting a moving object. Comparison inspections of these same elements are now being taken by other ultrasonic techniques and by radiographic methods.

b. Correlation of Heat Transfer and Bond Quality. The correlation between ultrasonic transmission capabilities of various types of mechanical bonds and their heat-transfer capabilities is being studied to determine the thermal properties of the bonds by the thermal-pulse method for measuring diffusivity and conductivity developed by Parker et al.[9] The front surface of the specimens are uniformly irradiated by a very short (approximately 600 μsec) pulse of radiant energy supplied by a xenon flash tube. The temperature history of the back surface is continuously monitored by feeding

[9] Parker, W. J., Jenkins, R. J., Butler, C. P., and Abbott, G. L., Flash Method of Determining Thermal Diffusivity, Heat Capacity and Thermal Conductivity, J. Appl. Phys. 32, 1679 (1961).

the output of a thermocouple in contact with the back surface into a differential amplifying system and then into an oscilloscope. Measurements of thermal diffusivity α and conductivity k of the copper braze-bonded specimens have been completed. Values of α ranged from 1.01 to 0.009 cm^2/sec, and of k from 0.882 to 0.008 cal-cm/cm^2-sec-°C. For copper α = 1.14 cm^2/sec and k = 0.922 cal-cm/cm^2-sec-°C. Ultrasonic tests on these specimens should be started in the near future.

Plans are being made to extend this study to diffusion bonds. It is hoped that suitable specimens can be made from fuel plates that have been rejected on the basis of the ultrasonic tests.

c. Neutron Radiography. Nuclear fuels, when tested in reactors, soon become so radioactive that they must be encapsulated before the start of a test. The removal of specimens from their capsules (for examination), followed by the re-encapsulation of the specimen for further irradiation, is complicated, time-consuming, and usually detrimental to the success of the experiment. It is therefore advantageous to follow the experiment by photographing images of the specimens and associated equipment in the capsule. A method of obtaining the images by neutron radiography has been developed. The study of phosphors for possible use in a neutron image converter has continued. A combination of Li^6F and ZnS is the most promising phosphor tested to date, and attempts to optimize the composition are now under way.

E. Remote Control Engineering Development

1. Viewing Systems

The program to develop better radiation-resistant glasses includes basic investigations of experimental glasses and accelerated performance tests with a variety of practical shielding glasses. The basic investigations are carried out in order to broaden the understanding of specific aspects of the problem and to give direction to the experimental tests on practical glasses. Current basic investigations pertain to the role that cerium and other additives play in the suppression of radiation induced coloration (see Progress Report for March 1964, ANL-6880, pp. 59-60) and to the glass properties that prevent fracturing produced by electrical discharge.

Thick castings of shielding window glasses in common use today have been found to be quite susceptible to fracture by electrical discharge if the surface is scratched or chipped. Preliminary studies (see Progress Report for May 1963, ANL-6739, pp. 45-47) were carried out with 4-inch cubes of glass. All commercial glasses tested were easily discharged by a small impact after an exposure of 1 to 10 megaroentgens. The impact or penetration of the surface required to initiate discharge decreased with increase in exposure. It is thought that the discharge is readily initiated

because of the high voltage gradient generated in the glass. This occurs in high-resistivity glasses as a result of the electrons freed in the glass by Compton scattering. Also, a serious effect for large windows is that a small fracture, once formed, will continue to grow with subsequent exposure.

The effect of increasing the excitation level in the glass by exposure to 10-MeV electrons from a linear accelerator is being studied. Immediately after exposure, a glass sample is chipped slightly to initiate discharge and the charge released is measured. So far, this test clearly distinguished between lead and barium silicate glasses. However, more tests are needed before the electron-irradiation results can be correlated with gamma-irradiation results. If the results can be correlated, the electron irradiation would aid in testing a considerable number of experimental glass compositions for relative susceptability to discharge. The samples required can be small enough to be easily melted and the exposure time is less than a minute per sample. Glass samples that show the least susceptability to discharge will be prepared in large samples for gamma irradiation.

2. Electric Master-Slave Manipulator Mark E4

A new 50-lb load-capacity, electric master-slave manipulator is being developed. The principal improvements over the existing Model 3 Manipulator are: (1) the manipulator slave arm will be able to approach work from many directions; (2) the master arms will be better suited to working with different types of viewing, such as windows, periscopes, and television monitors; (3) the slave arm motors will be cooled better so that they can work in higher ambient temperatures; (4) the electrical servo system is designed to allow the slave arms to be operated up to 2,000 ft from the master arms; (5) the manipulator will have higher dependability; and (6) the slave arm will be easier to repair, and much of the repair can be done remotely.

The reach and maneuverability of the present manipulator configuration would go a long way toward solving some of the problems in the cave over the FARET reactor, in the Alpha-Gamma Cave for Metallurgy, in the hot cells at the Nuclear Rocket Development Site, and would also have potential use for repairing other equipment, such as various components of high-energy particle accelerators.

The manipulator has seven master-slave motions. Each consists principally of a slave-arm servo drive unit, a master-arm servo unit, and a servo amplifier. Each slave servo drive unit will have a brake which can be set by the operator, or will automatically be set by a fail-safe circuit in case of an electrical malfunction.

The force capabilities of the slave arm in any direction is 0 to 50 lb, and the reflected force capabilities of the master arm vary from 0 to 17 lb.

The force fed back to the master arm and handle can be selected to be either equal to, or one-third of, the force at the slave arm for loads under 17 lb. Above 17 lb at the slave arm, the force fed back to the master arm and handle must be selected to be one-third of the force at the slave.

The servo drive units, consisting of motors, tachometers, synchros, and gearing, are the same for the new configurations as they were for the earlier telescoping configuration. The servo drive units and servo amplifiers have been nearly completed in design and some parts fabricated. A prototype servo amplifier has been tested with the servo drive units and the performance is satisfactory.

Several configurations of the arm have been studied and mockups of a number of these have been made. In addition, some hardware has been built in order to work out some of the mechanical problems. An earlier configuration utilized a telescoping lower arm. After considerable study of several of the detail problems, the telescoping design appeared undesirably complex. Other configurations have been investigated in an effort to decrease cost and/or gain a configuration which would be more useful in a wider variety of applications.

3. Special Motors for Master-Slave Manipulators

Two different low-inertia motors have been designed and are being fabricated for test and possible use in future electric master-slave manipulators having load capacities between 50 and 100 lb. The actual capacity of the manipulator will depend on the speed at which the slave arm moves and the amount of heat that can be removed from the motors. One of the motors is two-phase, 60-cycle, with a thin-walled aluminum cup rotor. It is designed with special laminations to provide air passages between the rotor and windings to remove the heat. The other motor has a permanent magnet for its rotor and has the commutated winding in the stator. This inverse (compared with conventional dc motors) arrangement allows for a much greater volume of conductor in the commutated winding and allows the rotor to have much lower inertia compared with conventional designs. There are no other known motors in this country of equal power with as high a torque-to-inertia ratio.

4. Telescopes and Periscopes for Use with Master-Slave Manipulators

Studies are being carried out on various parameters of telescopes and periscopes to determine the limitations of existing systems and the new characteristics required to make them useful for viewing by a manipulator operator performing work efficiently at distances between 15 to 100 ft. The parameters being studied include the effects of: exit pupil size, eye relief, sighting capabilities, and positioning methods. We have found that, because

of the normal head movements of a manipulator operator, it is desirable that the telescope or periscope have a relatively large exit pupil and eye relief.

5. Master Control Handle

Several design studies have been made of control handles for the master arm of master-slave manipulators in order to get better mechanical coupling between the operator's hand and the handle for all six of the basic motions and to get a convenient method of operating the tongs. Present handles have quite poor mechanical coupling of the operator's hand to the handle in two of the six motions.

6. Rotating Gas Seal for Manipulator Boot

A rotating "seal" which permits unsealed mechanical master-slave manipulators to be operated in an inert gas atmosphere has been developed and is being tested. This seal permits free rotation of the wrist and azimuth motions of the manipulator by allowing the lower portion of a boot to freely rotate with respect to the upper portion. The slave arm of the manipulator can be withdrawn from the seal for repair, and the lower boot can be remotely replaced.

7. Future "High Fidelity" Manipulators

Recent studies indicate that it is possible and practical to develop manipulator systems and special tools to the point that almost any equipment could be remotely repaired even though it was only designed for manual repair. The approach that seems most likely to yield substantial progress toward this goal, in a reasonable length of time, is to develop electric master-slave manipulators that have a much more accurate force feedback, so that the operator can get a dynamic feel reasonably similar to that which he feels when he holds a tool in his own hand. The present "medium fidelity" master-slave manipulators give force feedback, but this feedback does not extend into the higher frequencies and the accuracy of feedback at low frequencies is inadequate for sensitive operations.

The first several generations of these "high fidelity" manipulators would probably have only seven to ten independent master-slave motions and would necessarily need numerous special tools and wrenches. The rate of performing work would most likely be considerably below the rate of performing it directly with the hands.

Successful reduction to practice of manipulator systems having these "high fidelity" capabilities would open up new, less costly approaches to the design of reactor systems, reprocessing plants, hot laboratories, repair of nuclear rockets on earth and possibly in space, and repair of some future high-current high-energy accelerators.

F. Heat Engineering

1. Studies of Boiling Liquid Metals

Experimental information pertinent to the two-phase fluid dynamic and boiling heat transfer behavior of the alkali metals is being collected. The parameters of interest include two-phase pressure losses, variation of vapor volume fraction with pressure and quality, variations of boiling heat flux, overall condensation behavior, and boiling stability. These parameters will be varied over a wide temperature range extending to 2100°F, and most experiments will utilize sodium as the fluid medium in the forced-convection systems.

a. Void Fraction - Pressure-drop Facility. A forced-convection, boiling sodium loop, constructed of Type 316 stainless steel, has been designed to measure two-phase pressure losses (adiabatic) and vapor volume fraction in flowing sodium, and is limited to short-term operation at approximately one atmosphere and 1632°F. Construction of the loop is essentially complete, and calibration and fill procedures are underway.

The 10-kc eddy-current liquid level probes are being calibrated for sensitivity and temperature coefficient (which is very small). A highly stable, linear dc amplifier has been incorporated into the zero-point calibration circuit and the probe output circuit; this component has eliminated all the drift difficulties, and the level reading should be accurate to ±0.1 in. of liquid level.

Measurements of the effective electrical resistance of the electromagnetic flowmeters at various values of temperature and vapor volume fraction is expected to provide basic data for MHD experiments. Such simple measurements will not interfere with the primary measurement of void fraction and two-phase pressure losses.

Upon completion of the level-probe installations, the sodium fill process will be tested in the main loop, and the gas control system will be tested prior to the flowmeter calibrations.

2. Boiling Sodium Heat Transfer Facility

a. Niobium-Zirconium Loop Construction. Work during this past month centered on preparations for the installation of the vacuum chamber and related equipment. Some revision in the layout of the equipment was made to satisfy handling requirements for the liquid nitrogen to be used in the cold baffle on the chamber. Plans were also made for the procurement of liquid nitrogen (a manifold and piping system was designed) as well as for the supply and drain systems for the eleven cooling-water circuits

associated with the chamber and power equipment. Some flow-measuring temperature-measuring, and safety interlocking equipment was obtained for these circuits.

b. Heater Experiments. Refinements on the vacuum enclosure for housing the thermal-radiation-heated loop have been completed. The heater section has been welded into position, thus completing the loop assembly. Thermocouples have been located at various positions on the loop. The electromagnetic flowmeter is being calibrated.

Difficulties have been encountered in leak checking the system. The leak detector, presently being rebuilt, will soon be available.

3. Double-pipe Liquid Metal Heat Exchanger

A heat transfer loop is being designed to investigate heat transfer with mercury flowing cocurrently in a double-pipe heat exchanger. The loop will consist of a centrifugal pump, Calrod heater rated at 10 kW as the heat source, a water cooler as the heat sink, electromagnetic flowmeters for measurements of both the tube and annulus output flow rates, an expansion tank, dump tank, and the test section. The flow system, which will operate under maximum conditions of 80 psi and 200°F, is to be constructed mainly of stainless steel.

The main objective of the investigation is to obtain fully developed, local heat transfer rates as a function of the operating conditions of the exchanger. This is to be achieved by making a local temperature measurement in the wall of the center tube at the outlet of the exchanger. From the bulk fluid temperatures of the tube and annulus at the outlet, and from the overall fully developed heat transfer coefficient and the wall resistance, the tube wall surface temperatures may be calculated, and from these temperatures, the local coefficients may be determined.

The test section will be constructed of nickel in order to reduce the temperature gradients in the tube wall. A hydrodynamic entrance length of about 20 diameters in length will precede the heat transfer section of the test section which will be from 15 to 30 diameters in length with annular ratios of from 1.2 to 2.0.

Design is near completion.

4. ANL-AMU Program

Other heat engineering experiments, performed as part of a joint program (not supported by the Division of Reactor Development) between the Laboratory and the Associated Midwest Universities (AMU), are described below:

a. Transient Behavior of Heat Transfer Loop. In the Progress Report for March 1964, ANL-6880, p. 62, it was noted that the rapid (6-24 cps) oscillations which occur at bulk temperatures substantially below the thermodynamic critical point, were believed to be an acoustic type of pressure wave. A turbine-type flowmeter does not indicate flow fluctuations of the magnitude previously measured by means of a Venturi. Apparently, the oscillations of the Venturi pressure drop are caused by a pressure wave crossing the Venturi taps rather than as a result of flow fluctuations.

If the above speculation is true, one would suspect that the frequency of the oscillations should be a function of the fluid properties, since the sonic velocity decreases as the critical temperature is approached (theoretically it should equal zero at the critical point). If the wavelength remains constant (at a value which depends on loop geometry), then the frequency should also decrease as the critical temperature is approached according to the equation

$$f = C/\lambda,$$

where f is the frequency (cps), C the speed of sound (ft/sec), and λ = wavelength (ft).

In order to test this hypothesis, the experimentally determined frequency was plotted versus the average temperature in the system. Figure 10 shows the results for all presently tabulated data. The data for the

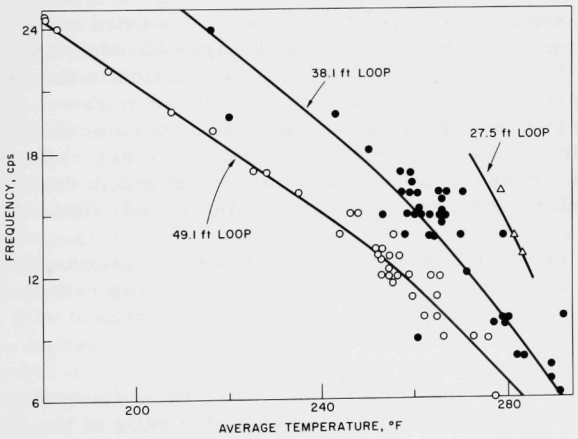

Figure 10. Frequency vs. Average Temperature in Several Loops

two shorter loops were taken from ANL-6710.[10] Two facts are evident. The frequency decreases with increasing temperature, as would be surmised from the behavior of the sonic velocity, which also decreases with temperature in the given region. The frequency is inversely proportional to the length of the loop for a given average temperature. Hence, we conclude that the sonic-type oscillations are of a resonant nature with a wavelength equal to the length of the loop. In several instances when the power was suddenly increased, the wavelength was only one-half the loop length. These isolated instances resulted in more severe pressure oscillations across the Venturi, as would be expected.

Attempts to measure the sonic velocity have not been wholly successful to date. However, the sonic velocity appears to be of the order of 700 ft/sec at a temperature 40-50°F below the critical. By use of this value, a resonant frequency of 14 cps would indicate a wavelength of 49 ft, which is equal to the length around the loop. This fact also tends to support the conclusion that the rapid oscillations are an acoustic type of phenomenon with a wavelength equal to the distance around the loop.

b. Two-phase Nozzle Flow Studies. The existing literature on two-phase nozzle flow has been critically examined. Considerably more information is available for two-component than for single-component two-phase flow in converging-diverging nozzles in the low-quality region. Although efficiencies and relative velocities between the phases in two-component systems have been reported, no direct information can be found for one-component systems.

Only one source of data could be located on one-component, two-phase flow through nozzles (ASME paper 63-AHGT-4). The thrust of the leaving fluid stream was measured in addition to the usual measurements of flow rate and pressure profile throughout the nozzles. Exit qualities ranged from 14 to 35 percent, based on equilibrium calculations. No attempt was made in this paper to measure or calculate slip ratio or efficiencies of the nozzles. These data were therefore examined in detail to obtain information on slip ratios, nonequilibrium effects, and efficiencies of the nozzles.

A two-phase nozzle test facility has been built from which exit qualities from 1 to 7 percent were obtained. Slip ratio measured at the exit of the nozzle ranged from 5 to 40, and increased with increasing quality.

The data indicate that the efficiency of a two-phase flow nozzle (the efficiency as used here is defined as the ratio of the actual kinetic energy of a unit mass of the leaving liquid phase to the kinetic energy of a unit mass of fluid expanding ideally) is a strong function of exit quality, and can be related to the various flow patterns occurring in the nozzle. At qualities below 1 percent, high efficiencies are indicated (bubble flow).

[10] D. G. Harden, Transient Behavior of a Natural-circulation Loop Operating near the Thermodynamic Critical Point, ANL-6710 (May 1963).

From 1 to 10 percent quality, the efficiency is decreasing for increasing quality (slug, annular flow), and efficiencies as low as 1 percent can be expected. Above 10 percent quality, the efficiency is found to increase sharply (dispersed flow), and the data examined indicate that a properly designed nozzle can give efficiencies as high as 90 percent.

The data available on two-component systems have been compared with the data from the one-component system and show similar trends. The latter system, however, was complicated by nonequilibrium effects.

c. Inception of Instability in a Natural-circulation Loop. The redesigned Armadilla Loop was completed and a pressure test up to 3000 psi showed no weakness. However, heating of the test section indicated a need for a strong shroud in order to prevent buckling. The shroud is being added.

At this time, instrumentation for the loop is being prepared, and it is hoped that the loop will be ready for operation within two weeks.

d. Power-to-void Transfer Functions. Dynamic data are now being provided by the experimental investigation of power-to-void transfer functions. Several small changes have been made in the Small Scale Loop, namely the installation of a new Pottermeter and also a low-flow power trip to prevent burnout from loss of flow. The test sections have been received and all dimensional tolerances were excellent (±0.002 in.).

All electronic equipment has been functioning properly, including the new Analog Computer which has been built to replace borrowed equipment. The new 8-channel recorder is being used satisfactorily for determining system parameters.

To date, measurements of the void response to power modulation in the frequency range from 0.01 to 10 cps have been made at 400 psia. It is planned to shake down the equipment and also to analyze fully the power-to-void transfer function at this pressure before proceeding to higher flow rates and pressures. The data cover measurements at various axial positions along the channel. Investigations are planned for various transverse positions of the channel.

The digital computer program is being used to generate theoretical curves with which the experimental data can be compared. The two-phase flow models or quality-void fraction relationships which are presently being used are those of Marchaterre-Hoglund[11] and Bankoff.[12]

---

[11] J. Marchaterre and B. M. Hoglund, Nucleonics, 20 142 (Aug 1962).

[12] S. G. Bankoff, J. Heat Transfer, 82 (Series C) 65 (Nov 1960).

Future work includes instrumentation of the new test section and its installation in the loop. Also, final designs are being completed for the new power shunt, and completion is scheduled for April 30. Since both of the above projects do not interfere with operation of the loop, the experimental investigation will be continued.

G. Chemical Separations

1. Chemistry of Liquid Metals

From measurements of the equilibrium pressure of cadmium over the two-phase region LaCd-La and previous equilibrium pressure measurements (see Progress Report for February 1964, ANL-6860, p. 75), the free energies of formation of LaCd and of the other lanthanum-cadmium intermetallic compounds, $LaCd_2$, La_3Cd_{13}, and La_2Cd_{17}, are being evaluated. At 450°C, the free energy of formation of $LaCd_{11}$ is found to be -43.0 kcal/mole, which agrees well with the value of -40.8 kcal/mole determined by use of the galvanic cell (see Progress Report for December 1963, ANL-6810, p. 36).

2. Fluidization and Volatility Separation Processes

a. Recovery of Uranium from Low-enrichment Ceramic Fuels. Laboratory work in support of the pilot-plant study of a fluid-bed fluoride volatility process is directed toward determining the optimum conditions for the fluorination of U_3O_8-PuO_2 mixtures in a fluidized bed of alumina granules and for the efficient removal of plutonium from the fluid bed.

Alumina granules from a fluid-bed which had been used for the fluorination of a U_3O_8-PuO_2 mixture were examined by an autoradiographic method[13] to determine whether plutonium retained by the alumina is on the surface of the alumina granule or dispersed through the body of the alumina granule. In the autoradiographic method, the alpha activity of the plutonium is used to indicate its location on (or in) the alumina particles. In the developed photographic emulsion, the tracks produced by the alpha particles are readily distinguishable from the general darkening that is produced by beta radiation. (This technique has been used in the Chemical Engineering Division to determine the location of the site of plutonium in a metal matrix.) The results of these tests clearly showed that the plutonium is present as a layer on the surface of the alumina granules.

As a means of obtaining better removal of plutonium from alumina in laboratory-scale studies of the fluid-bed fluorination of U_3O_8-PuO_2 mixtures (see Progress Report for March 1964, ANL-6880, p. 64), the use of an additive compound which would increase the fluorination rate of uranium and plutonium was examined. Bismuth trifluoride is being considered as the additive compound. It reacts with fluorine to form bismuth

[13] M. D. Adams and R. K. Steunenberg, Some Metallurgical Applications of Autoradiography, ANL-6412 (Oct 1961).

pentafluoride, a strong fluorinating agent,[14] which in turn might be expected to increase the rate of fluorination of uranium and plutonium. In the present studies, the effect of the addition of BiF_3 upon the fluorination rates of U_3O_8 and UO_2F_2 was determined by means of thermobalance. The conditions and the results of the fluorination experiments are shown in the following:

Material	Temperature[a] (°C)	Fluorination[b] Rate (mg/min)
BiF_3	400	0.4
UO_2F_2	400	4
10 w/o BiF_3-90 w/o UO_2F_2	400	3.5
30 w/o BiF_3-70 w/o UO_2F_2	400	2.3
BiF_3	450	2
U_3O_8	450	2
7.5 w/o BiF_3-92.5 w/o U_3O_8	450	6-8
15 w/o BiF_3-85 w/o U_3O_8	450	14

[a]Temperature as indicated, ±10°C.
[b]Fluorine flow: 200 cc/min.

The results showed that the fluorination rates for UO_2F_2 decreased with the addition of BiF_3 at 400°C and that the fluorination rates for U_3O_8 increased with the addition of BiF_3 at 450°C.

b. Recovery of Uranium from Highly Enriched Uranium-Alloy Fuels by Chlorination and Fluorination Steps

(i) Laboratory-scale Studies. Development studies have continued on a fluid-bed chlorination-fluorination process for the recovery of enriched uranium from uranium-alloy fuels. Experimental tests are being carried out with uranium-aluminum and uranium-Zircaloy fuels in a $1\frac{1}{2}$-in.-diameter fluid-bed reactor with the alloy submerged in an inert bed of alumina particles. Data from 39 previous experiments were evaluated by a stepwise multiple regression analysis to aid in defining the effects of operating variables on uranium retention on the alumina bed material after fluorination. The results indicate that those operating conditions which tend to lower the partial pressure of UF_6 in the gas stream during fluorination result in lower retention of uranium by alumina. Lowering of the bed temperature to 250°C during the initial stages of the fluorination resulted in lower fluorination rates and hence lower partial pressures of UF_6 with a concomitant lowering of the amount of uranium retained by the alumina (see Progress Report for February 1964, ANL-6860, pp. 76-77).

(ii) Pilot-plant Demonstration Tests. Six preliminary tests have been completed in the pilot-plant facility that has been installed to

[14] J. Fischer and E. Rudzitis, J. Am. Chem. Soc., 81, 6375 (1959).

demonstrate the recovery of uranium from enriched uranium alloy fuels by fluid-bed fluoride volatility techniques. Three tests involved assemblies of Zircaloy plates and three were with assemblies of aluminum plates. These tests, which demonstrated only the hydrochlorination and hydrofluorination steps of the process, were useful in establishing processing conditions for both steps (see Table XXIII). The data in Table XXIII are not considered optimum, but represent the processing conditions which resulted in very satisfactory operation of the pilot-plant facility. The hydrochlorination temperatures are 50 to 100°C higher for the Zircaloy-based fuels, with the alumina bed material maintained at 450°C for Zircaloy fuels and 350°C for aluminum fuels. The hydrofluorination processing conditions are identical for both types of fuels. Hydrogen chloride utilization efficiencies of 50% or greater were obtained for batch charges of either fuel type without hydrogen chloride recycle.

Table XXIII. Processing Conditions for Pilot-plant Tests

Equipment: Main reactor - 6-in.-diameter nickel reactor containing 40 kg granular alumina; packed-bed filter - 9-in.-diameter unit containing 9 kg granular alumina as filter media; pyrhydrolysis reactor - 6-in.-diameter stainless steel reactor containing 20 kg bed material.

Processing Parameters	Fuel Material	
	Zircaloy Fuel, PWR Type	Aluminum Fuel, MTR and ETR Type
I. Hydrochlorination		
A. Typical Charge		
Weight (kg)	20	7
No. Plates	14	19
Length (in.)	48	36
Uranium (g)	180	280
B. HCl Concentration (v/o)	70	80
C. Gas Velocity in Reactor (ft/sec)	0.6	0.6
D. Process Temperatures (°C)		
Reactor Bed	450	350
Reactor Wall	350	275
Packed-bed Filter	350	200
Pyrohydrolyser	350	300-350
E. Reaction Rate (kg/hr)	2.0-3.0	1.5-2.0
HCl Utilization (%)	50	60
Reaction Time (hr)	7-10	4-5
F. Inert Bed Material		
Reactor Bed	Alcoa T 61 Alumina, 28-100 mesh	
Packed-bed Filter	Alcoa T 61 Alumina, 14-28 mesh	
Pyrohydrolyser	Sand, 20 to 40 mesh	
II. Hydrofluorination		
A. HF Concentration (v/o)	20	
B. Gas Velocity in Reactor (ft/sec)	0.5	
C. Process Temperatures (°C)		
Reactor Bed	350	
Packed-bed Filter	350	
D. Reaction Time (hr)	2.0	

c. Corrosion Studies. Corrosion studies in support of the fluid-bed fluoride volatility programs for both high-enriched and low-enriched fuels are in progress. The main aim of these studies is to determine whether nickel is suitable as a material of construction. The first series of tests in which nickel-200 and welded specimens of nickel-200 were exposed to simulated process environments have been completed. The results of the test are given in Table XXIV. Each value shown represents an average of four specimens evaluated after exposure time of 240, 480, or 960 hr.

Table XXIV. Corrosion of Nickel Plate and Welded Nickel

	Corrosion Rate, mils/yr								
	Nickel-200 Plate[d]			61 Filler Metal Welds[e]			Nickel-200 Welds[f]		
Environment	240 hr	480 hr	960 hr	240 hr	480 hr	960 hr	240 hr	480 hr	960 hr
F_2 at 475°C[a]	0.9	0.9	0.9	1315	763	695	2.0	3.4	0.6
F_2/HCl at 450°C[b]	2.1	1.5	0.9	67	76	70	3.3	2.2	1.1
F_2/O_2 at 500°C[c]	1.9	3.8	4.1	382	673	707	5.0	4.4	2.2

[a]Specimens were held at 475 ± 35°C in an atmosphere of 50 v/o fluorine in nitrogen at about 1000 mm Hg absolute. Total flow rate was about 50 ml/min at NPT (once-through).

[b]Specimens were held at 450 ± 10°C in an atmosphere of 50 v/o fluorine in nitrogen, alternated with an atmosphere of 50 v/o HCl in nitrogen every 24 hr. Flow conditions were similar to those listed in footnote "a" above.

[c]Specimens were held at 500 ± 25°C in an atmosphere of 50 v/o fluorine in nitrogen, alternated with an atmosphere of 50 v/o oxygen in nitrogen every 24 hr. Flow conditions were similar to those listed in footnote "a" above.

[d]Nickel-200 plate, thicknesses 1/16 and 1/8 in., manufactured by the International Nickel Co., Inc., and having the following nominal composition in percent: Ni, 99.5; C, 0.06; Mn, 0.25; Fe, 0.15; S, 0.005; Si, 0.05; and Cu, 0.05.

[e]These specimens were made of two pieces of nickel-200 plate, 3/16 in. thick, welded together with nickel filler metal 61. The filler metal has the following nominal composition in percent: Ni, 93.0; C, 0.15; Mn, 1.0; Fe, 1.0; S, 0.01; Si, 0.75; Cu, 0.25; Al, 1.50; Ti, 2.0-3.5; other, 0.50.

[f]These specimens were made of two pieces of nickel-200 plate, 3/16 in. thick, welded together with nickel-200 filler metal.

The corrosion rates for the fluorine-hydrogen chloride environment and fluorine-oxygen environment were found to be somewhat higher than the 50 v/o fluorine environment, but the range of values (0.9 to 4.1 mils/yr) indicates that only a small change in the corrosion rate occurs by alternating a fluorine environment with either hydrogen chloride or oxygen. This change is regarded as being small with reference to the values that are regarded as being acceptable as corrosion rates (20 to 50 mils/yr) for nickel in plant use. Metallographic examination of the specimens after exposure disclosed no evidence of intergranular penetration.

A comparison of the values for the corrosion rate of nickel-200 welded with filler metal 61 and nickel-200 welded with nickel-200 filler

shows clearly that the nickel-200 filler has superior corrosion resistance in every instance (see Progress Report for March 1964, ANL-6880, p. 65). The corrosion rate for welded specimens was calculated by determining the weight loss after defilming and assuming that this loss occurred uniformly over the original weld area.

Some caution is required in applying these results to plant conditions, since consideration must be given to factors such as thermal cycling, which may significantly alter the corrosion rate of plant equipment. A series of tests are being made in which the effect of thermal cycling on the corrosion resistance of nickel will be evaluated.

3. General Chemistry and Chemical Engineering

a. Preparation of Magnesium Sesquicarbide. One of the methods being evaluated for the preparations of UC and (U-Pu)C solid solutions is the reaction of Mg_2C_3 with uranium salts or uranium-plutonium salts dissolved in a fused salt mixture, such as LiCl-$MgCl_2$. The Mg_2C_3 which has been used for these reactions was prepared by the direct reaction of magnesium metal with pentane gas.

A modified preparative method for Mg_2C_3 is being examined. Pentane gas is passed through a molten zinc-magnesium alloy which contacts a LiCl-$MgCl_2$ melt held at about 640°C. Magnesium carbide is formed in the alloy phase, but goes into solution in the salt phase. It is proposed to separate mechanically the magnesium carbide-bearing salt phase from the alloy. This salt phase is then added to a similar salt phase containing uranium or uranium-plutonium, and, upon heating, the uranium and plutonium carbides are expected to form.

Two preparations of magnesium carbide were made in the system zinc-50 w/o magnesium and $MgCl_2$-35 m/o LiCl; samples of the final salt phases were analyzed for carbide by hydrolyzing the salt in a closed system and measuring the volume of gas evolved. (MgC_2 upon hydrolysis yields acetylene and Mg_2C_3 yields methyl acetylene.[15]) If one assumes that the gas evolved by hydrolysis of salt from the first preparation was only methyl acetylene, the Mg_2C_3 content of the salt phase was only 0.4 w/o. For the salt sample from the second preparation, not only was the volume of gas measured, but also the molecular weight of the gas was determined by the vapor density method. From the molecular weight data and gas volume, the salt composition was calculated to be 2.2 w/o MgC_2 and 3.9 w/o Mg_2C_3. These results are encouraging, and additional preparations of magnesium carbide are being made in an effort to obtain better yields.

---

[15] Sidgwick, N. V., The Chemical Elements and Their Compounds, Vol. 1, Oxford University Press, London, p. 223.

4. Calorimetry

Fifteen calorimetric combustions of silicon carbide in fluorine have been performed. Two samples of alpha silicon carbide and two samples of the beta variety were utilized in these experiments. Preliminary calculations show no significant difference for the two crystalline modifications. The tentative values for standard energy change per gram of sample at 25°C, ΔE_c°, were -14,698.09 ± 0.2 cal g^{-1} for alpha silicon carbide and -14,700.21 ± 4.2 cal g^{-1} for beta silicon carbide.

Seven calorimetric combustions of magnesium in fluorine and seven calorimetric combustions of yttrium in fluorine have been completed. Tentative values for the standard energy change per gram of magnesium and yttrium sample are -11,028 ± 6 cal g^{-1} and -4609.8 ± 4.0 cal g^{-1}, respectively.

H. Plutonium Recycle Program

1. Plutonium Recycle Experiment

The safety analysis for the Plutonium Recycle Experiment has been transmitted to the AEC for review. The analysis considers the case where any water penetrating cracks in the cladding remains in the interior of the fuel pin. Calculations were made of the effects of this "waterlogging" on reactivity, assuming that ten percent of the volume of all the fuel pins is water. The results showed that "waterlogging" would not cause a noticeable change in reactivity in the critical experiment and that it would cause a decrease of 0.3% in reactivity in the full system.

The effect of void concentration on the buildup of plutonium isotopes was also investigated. CYCLE calculations based on average plutonium zone voids of 0.2, 0.3, and 0.4 and the relative voids in plutonium, 1st shim, 2nd shim, and uranium zones were taken to be in the ratio of 1.0/1.0/1.0/0.5. The deviation in the plutonium isotopic concentrations relative to the void fractions as a function of burnup are given in Table XXV. The influence of the void distribution on the concentration of plutonium isotopes is small.

Table XXV. Deviation in Percent for Various Isotopic Concentrations Relative to 0.3 Plutonium-zone Void Fraction

	Pu^{239} Plutonium-zone Void		Pu^{240} Plutonium-zone Void		Pu^{241} Plutonium-zone Void	
Burnup	0.4	0.2	0.4	0.2	0.4	0.2
0	0	0	0	0	0	0
0.00075	0.3	-0.2	-0.5	0.4	5.8	-4.8
0.0015	0.7	-0.5	-0.9	0.6	5.4	-4.4
0.0030	1.6	-1.1	-1.4	1.0	4.6	-3.8
0.0045	2.5	-1.8	-1.6	1.2	3.9	-3.3
0.0060	3.6	-2.6	-1.6	1.2	3.4	-2.9

Hydrodynamic instrument response in previous EBWR cores showed that local voids cannot be checked to better than ±0.1. Accordingly, instruments will not be included in the downcomer for the Plutonium Recycle Experiment.

2. Pressure Vessel Steel

Part of the EBWR Plutonium Recycle Program consists of irradiation surveillance of the pressure vessel steel. Experimental work contributory to the surveillance program has been performed as noted below.

Mechanical, magnetic, and resonant properties of EBWR vessel steel which was irradiated as MTR-ANL-26 have been measured. Similar data have been collected for two different heats of SA-212 B, known as pedigreed steel, which was irradiated in EBWR. A third set of data was obtained from stressed SA-212 B pressure vessel steel,samples of which were taken from the EBWR at the time of the conversion of the facility for 100-MW operation. Examination of the data revealed that the SA-212 B pedigree heat of steel is substantially different from the EBWR pressure vessel steel in one significant property, i.e., resistance to impact. As a consequence, the next irradiation surveillance of the EBWR will be on EBWR pressure vessel steel to provide the missing link (if any) to connect the three sets of data. Additional SA-212 B data (from the SL-1 pressure vessel) will be incorporated into this study.

Another portion of the recycle preparation program consists of examination of piping by nondestructive techniques with confirming sectioning of any suspicious areas. Only one of five commercial NDT inspection laboratories has shown an interest in the field examination of the EBWR piping and a preliminary cost estimate is being prepared. This company is experiencing difficulties in procuring piping materials for the preparation of reference standards for ultrasonic testing.

IV. ADVANCED SYSTEMS RESEARCH AND DEVELOPMENT

A. Argonne Advanced Research Reactor (AARR)

1. Core Physics

Flux and power distributions in polar coordinate (r-θ) geometry were obtained for a cylindrical core with 60° symmetry. Symmetry boundaries are at rod followers and the bisectors. The azimuthal variation in power, maximum to average, is 1.16 in the worst case. Currently underway is an investigation of the flux and power distribution with control rods in.

As part of the r-θ problem, fluxes in the reflector were determined for the case in which part of the flux-enhancing water gap between the inner and outer reflectors is replaced by beryllium.* Epithermal fluxes in the all-beryllium* reflector were 1.5 to 2 times those in the Be-H_2O configuration, and the thermal flux was down by a factor of 2. This demonstrates how simple modifications of the reflector can significantly alter the neutron-flux spectrum locally. For example, an experimenter could obtain an epithermal-neutron beam by such a modification of the reflector in front of his beam tube, while fluxes and spectra in other beam tubes would be unaffected.

The effect of natural samarium addition on k_{eff} has been determined. It is found that k_{eff} varies with the ratio R (R = number of natural samarium atoms added/number of U^{235} atoms present) in the range $0.016 \leq R \leq 0.046$ as

$$k_{eff} = 1.191 - 5.799\ R + 35.3251\ R^2.$$

Tentatively, it is planned to use natural samarium as a burnable poison.

Recovery from complete shutdown is governed by the amount of reactivity held down by rods as opposed to the increment held down by Xe^{135} (and Sm^{149}). At 100 MW the latter amount was a maximum of 3 percent Δk. A careful analysis of the xenon and samarium distribution at quasi-static equilibrium was made. It was found that, because of spatial variations in spectrum and power density, the xenon buildup following shutdown is not uniform. After 11.2 hr shutdown, the xenon is maximum in the inner high power region and the total increment in reactivity loss is 6 percent Δk.

---

*In all cases, the beryllium does contain a small amount of water in cooling channels, despite the "all-beryllium" design.

A CDC 3600 code is being developed to determine the concentrations of Xe^{135} and Sm^{149} in a reactor at various times after startup or shutdown.

2. Shielding and Preliminary Safety Analysis

Calculations for direct gamma-ray exposure for the AARR preliminary safety analysis were completed for a fission product release of 100% of the noble gases, 50% of the halogens, and 1% of the solids. This release is assumed to represent the condition subsequent to reactor operation at 240 MW for 37 days. If it be assumed that the fission products released above the main floor amount to 70% of the total, the radii of the exclusion area and low population zone are 550 and 850 m, respectively. These radii are reduced to 500 and 700 m when ventilation (at 100 cfs) and washdown are initiated at shutdown. In the latter case, 100% of the gases and 50% of the halogens and the solids (based on the source above the main floor) are assumed to enter the stack exhaust, and 25% of the halogens and the solids are assumed to be washed down to a shielded area at shutdown.

With filters in the exhaust system, exposure of the general public can be reduced well below statutory limits for accidental release. The direct gamma-ray dose requires a shielding wall to protect personnel near the reactor site. This wall (of ordinary concrete) need be only 12 to 18 in. thick; it is estimated that a 12-in. wall is needed for crane supports. Lining of the dome need not be so thick: for example, 6 to 9 in. is sufficient.

3. Fuel and Core Design

A hydraulic test loop is to be constructed for use in the AARR research and development program. The loop will be designed to circulate 200 to 800 gpm of light water in the temperature range from 100 to 500°F with a total pressure drop for 500°F water of about 250 psi. The maximum pressure of the closed system is limited to 1250 psig.

The loop will be used to investigate design problems caused by the high velocities and high power operation. These problems can be solved by experimental means more expeditiously and with greater accuracy than by analytical means alone. This is especially true with regard to fuel plate and fuel assembly integrity, since an analytical approach to determining strength characteristics still requires experimental measurements and verification for a given solution.

The loop will be used in the AARR Hydraulic-Structural Testing Program to study the following:

1. Determination of the effect of high-velocity flow across parallel plates with regard to structural strength, vibration, amplitude of vibration, flow distribution, and manufacturing tolerances on the fuel plates. This work will bring analytical design approaches closer to proper solution and provide experimental verific

2. Effect of thermal expansion on the hydraulic-structural characteristics of AARR fuel assemblies. This phase of the program will study the effect of thermal stresses caused by thermal expansions.

3. Effect of high-velocity flow and pressure differentials on sections of the core structure and on control blades. This phase of the work will prove the adequacy of the designed equipment.

4. Establish criteria for acceptance of fuel assemblies and formulate procedure and techniques for acceptance tests. This work will aid in specifying the functional requirements of the fuel assemblies expected of fuel assembly manufacturers.

5. The facility will be used for initial acceptance tests of AARR fuel assemblies that will be used in the reactor.

An analysis of stresses induced by both flowing fluid and temperature gradient in fuel plates of an AARR close side plate assembly has been started.

Since the finite Fourier transform cannot be applied directly to fuel plates with fixed edges, stress and deflection must be obtained by substituting an equivalent system. For example, a solution for stress and deflection can be obtained for two simply supported plates, each loaded differently, and superimposed. In this substitute calculation, one plate is loaded hydrodynamically and subjected to a bending moment at the fixed edges while the other plate is loaded with a different hydrodynamic load and subjected to a thermal load similar to that applied to the single plate system. The finite Fourier transform can now be applied to the superimposed plates to obtain a solution for the stress and deflection which could be expected in an AARR fuel plate.

B. Magnetohydrodynamics (MHD)

1. MHD Power Generation - Jet Pump Studies

Measurements of thrust and ejection rate were made on the compound nozzle referred to in the Progress Report for March 1964 (ANL-6680, p. 71). The measured velocity ratios from outer to center nozzle averaged approximately 1, 1.4, and 2. These figures are not exactly optimum for the operation, but it has been decided to try the operation of the jet pump. A preliminary nonoptimized operation of the loop has shown superior performance with this combination. The flowrate increase was measured at 25% higher than optimum for the single nozzle. However, the system feed steam pressure was found to be lower than desired so that modification of the inlet lines has been started to allow higher pressure operation.

During the thrust measurements, considerable electrification was observed in the area where the studies were being carried on. With proper arrangement of the jet and collector electrodes, it was discovered that an electrohydrodynamic (EHD) power unit could be operated. Measurements showed that about 80 J of 25,000-V electricity could be collected in 2.5 min. However, overall efficiency of the unit was very small. The phenomenon apparently seems to be caused by colliding of the jets to form a shock condensation zone with resultant entrapment of the positive charges in the steam cloud. Investigations of this approach have been discontinued.

2. MHD Vapor Condenser

The second stage of an analytical study of an electromagnetically controlled metal vapor condenser (see Progress Reports for May 1963, ANL-6739, p. 59, and August 1963, ANL-6780, p. 54) has been started. It was proposed that an electromagnetic field be utilized to pump condensed vapor off a condenser surface, thus increasing heat transfer rates and eliminating the necessity of gravity. The preliminary analysis indicated that condensation rates for typical metal vapors could be increased by factors of two to six; however, the analysis neglected ohmic heating in the condensate film.

A slightly more sophisticated model fully incorporates ohmic heating effects. Numerical results from this model are now being obtained.

V. NUCLEAR SAFETY

A. Thermal Reactor Safety Studies

1. Metal-Water Reactions

a. Reaction of 6061 Aluminum Alloy with Steam. Studies of the isothermal reaction of 6061 aluminum with steam (see Progress Report for March 1964, ANL-6880, p. 72) were continued as a part of a program to accumulate data that will allow a more direct comparison between results of laboratory experiments, data obtained in TREAT experiments, and results of reactor meltdowns. The 6061 aluminum alloy was the base alloy used in the SPERT-ID core. Of major interest in this study is the effect of the 6061 aluminum alloying elements (1% magnesium, 0.6% silicon, 0.25% copper, and 0.25% chromium) on the aluminum-steam reaction. The levitation method (see Progress Report for January 1964, ANL-6840, p. 92) is being used in these studies.

Preliminary results indicate that the reaction at 1500°C follows a cubic rate law. In this respect, the 6061 aluminum-steam reaction is similar to the reaction of aluminum-17 w/o uranium (SL-1 composition), which also follows a cubic rate law at 1500°C. However, the data indicate that the rate of the 6061 aluminum-steam reaction may be higher than the rate of the reaction of aluminum-17 w/o uranium with steam.

b. Reaction of Stainless Steel with Steam. Studies of the isothermal reaction of 304 stainless steel with steam have indicated that the initial rate of reaction depends upon the time required to heat the stainless steel sample to the test temperature in the presence of steam (see Progress Report for September 1963, ANL-6784, p. 65). The method used in these studies depended upon the measurement of the hydrogen evolved during the course of the reaction. When stainless steel was heated to 1300°C in the presence of steam, considerably higher rates of hydrogen evolution were obtained during the first 15 min of the reaction when the heatup time was 3 min, than the rates obtained in experiments in which the heatup time was 4 to 5 min. After 15 to 40 min, the rates of hydrogen evolution were the same in all tests.

Metallographic examination of four stainless steel samples used in these studies has been completed. The heat treatments to which the four samples were subjected were as follows: Samples 1 and 2 were heated to 1300°C in 5 min; Sample 1 was then cooled rapidly to room temperature, whereas Sample 2 was held at 1300°C for 30 min. Samples 3 and 4 were heated to 1300°C in 3 min; Sample 3 was then quenched to room temperature, whereas Sample 4 was maintained at 1300°C for 30 min.

A protective coating was formed on each sample. The coating was mainly metallic and possessed an enhanced concentration of nickel and chromium. Preliminary measurements indicated that the composition of the surface coating was 33 a/o Ni, 25 a/o Cr, <1 a/o Mn, 40 a/o Fe, and only 2 a/o oxygen (obtained by difference). The nominal composition of the original 304 stainless steel was 11 a/o Ni, 19 a/o Cr, <1 a/o Mn, and 70 a/o Fe.

The extent of formation and condition of the coating depended on the heat treatment to which the samples were subjected. The surfaces of Samples 1 and 2 were nearly completely covered by the coating. However, the coating of Sample 2, which was heated at 1300°C for 30 min after the 5-min heat-up period, was thicker than that of Sample 1, and showed some evidence of cracking. Sample 4, which was heated to temperature in 3 min and maintained at 1300°C for 30 min, had a coating that was similar to that of Sample 4, but was deeper in some areas. Sample 3, which was heated to temperature in 3 min and then quenched, was only coated in isolated areas. It is believed that the higher reaction rates observed initially in the samples that were more rapidly heated to the test temperature are due to incomplete formation of the coating, since the coating would be expected to be more resistant to reaction with steam owing to its higher nickel and chromium content.

c. Thermal Decomposition of Steam in a Flow System. Studies are being made of the thermal decomposition of steam resulting from the flowing of steam over heated metals. These studies are of importance to the understanding of the nature of events occurring in a reactor during a violent nuclear excursion. Experiments have shown that considerable knallgas ($2H_2 + O_2$) is produced when steam is passed over platinum at temperatures between 1275 and 1625°C. With flow rates of steam of 10 and 34 liters/(min)(cm^2 of cross section) over 1-cm platinum cubes, the rates of decomposition of steam were about 10^{-5} and 10^{-4} mole/(min)(cm^2 of Pt) at 1300 and 1600°C, respectively. In tests performed with readily oxidizable metals, such as molybdenum, rhenium, tungsten, tantalum, niobium, and zirconium, only hydrogen was produced. The less readily oxidizable metal, nickel, gave 3 to 10% oxygen in hydrogen over the temperature range 1300-1425°C.

The decomposition of steam by heated platinum is to be studied further to determine whether the reaction is catalytic or thermal.

d. Calculation of Pressure History of Reactor during an Excursion. A series of calculations have been undertaken of the transient heat transfer and pressure buildup occurring during a violent nuclear excursion. The initial calculations are designed to evaluate the rate of buildup of steam pressure by heat transfer alone. Attempts are being made to simulate mathematically the observations recorded during the final destructive test

of the SPERT-ID core. The simplifying assumptions are made that a uniform steam film is generated at the core surface and that there is a linear temperature gradient across the film at all times. The latter assumption leads to results that are numerically equivalent to the results generated by a more complex treatment, devised by Hamill and Bankoff,[16] as long as the steam film pressure does not approach the critical pressure (3200 psi).

An equation has been developed that describes the acoustic constraint that existed for 2 msec (the sonic loading time for the water column above the reactor). This equation was solved simultaneously with an equation for the energy balance over the steam film by a stepwise numerical method. Following the initial 2-msec period, the energy balance equation was solved simultaneously with an equation for the motion of the water column. The results reproduced the initial (35 psi) pulse measured in the SPERT reasonably well and indicated that the water column rose approximately 0.55 mm (maximum steam film thickness, 0.18 mm). The water column then descended, reaching a minimum at the time corresponding to the experimental beginning of the large destructive pressure rise. At this point the steam film thickness had decreased to 0.12 mm and the pressure was 2 atm. It is tentatively concluded that the decreasing film thickness and the rising pressure led to the disruption of the molten regions of the core, causing the rapid generation of steam. Calculation of the pressure generated by the newly created surface will be made, with an allowance included for the compressibility of the vapor generated prior to the disruption of the core.

The effect of hydrogen production by metal-water reactions will also be considered in future evaluations.

2. Metal Oxidation-Ignition Studies

Studies of the ignition temperatures of uranium-30 a/o plutonium ternary alloys were continued (see Progress Report for December 1963, ANL-6810, p. 50 and Progress Report for February 1964, ANL-6860, p. 94). These studies are being carried out to find an alloy of suitable composition for zero power critical experiments. Ignition studies with uranium-30 a/o plutonium-6 a/o iron alloy indicated that the ignition temperature is dependent upon the procedure used to prepare the sample. A chill-cast sample did not ignite in dry air even when heated to 820°C; in moist air, the sample ignited at 300°C. Injection-cast samples ignited at temperatures between 240 and 300°C. From these and previous results it is concluded that the addition of 6 a/o iron offers only a slight increase in the resistance of the alloy to ignition. Study of the ignition behavior of a uranium-18 a/o plutonium-14 a/o iron alloy indicated that this alloy does not offer an advantage over the binary uranium-18 a/o plutonium alloy or over the ternary alloy containing 6 a/o iron.

---

[16] T. D. Hamill and S. G. Bankoff, Chem. Eng. Sci., 18, 355 (1963).

Ternary alloys of uranium-30 a/o plutonium-6 a/o molybdenum were found to be less sensitive to the method of fabrication and to the presence of moisture. Self-heating was evident at 300°C, but ignition did not occur until the sample was heated to 600°C.

B. Fast Reactor Safety Studies

Two of the most important factors influencing the safety characteristics of fast power reactors are the large quantity of fuel and the short prompt-neutron lifetime. Therefore, it is possible to postulate a class of "meltdown" accidents, consisting of multistage incidents proceeding as follows: (1) some operating abnormality occurs in which the fuel undergoes failure, (2) material movements occur, which produce a more reactive configuration, and (3) a destructive burst of nuclear energy terminates the accident. The mechanisms involved in fuel failure and the material movement are complex. They are being studied experimentally in a program centering on tests being performed in the TREAT reactor.

1. Uranium-Thorium Fuel

Fully enriched U-20 w/o Th alloy fuel is of potential interest in fast reactors because of the superior dimensional stability under high temperature, long burnup, and steady-state irradiations, and because the Th-U^{233} breeding cycle for fast reactors may provide a reactor system having a sodium void coefficient less positive than those calculated for large uranium-plutonium breeder reactors. Approximately 75 cm of EBR-II size, thorium alloy has been obtained and will be used at first for a survey into modes of failure of sodium bonded, steel-clad EBR-II-type pins. Direct extrapolation of previous results on EBR-II samples does not appear to be justified since this alloy melts at about 1500°C. A liquid phase is indicated for temperature above 1080°C, so the failure mechanisms may be complex.

2. Photographic Experiments with Pre-irradiated Samples

The first four transparent meltdown capsule assemblies with pre-irradiated fuel samples have been disassembled by means of the remote equipment and techniques developed for the purpose. Post-experiment photographs have been taken of the fuel residue and test capsule interior, and samples have been carefully selected for chemical, metallographic, and gravimetric analysis.

3. Estimates of Maximum Transient Pressures

The approximate analytic and computer models developed earlier (see Progress Report for December 1963, ANL-6810, p. 53) for description of transient pressures and coolant expulsion in channels containing vaporizing coolant were used to estimate maximum transient pressures

in coolant channels sufficiently long so that pressure is limited only by the amount of power entering the coolant. For this condition, pressure increases until the rate of increase of the vapor-filled volume is so large that the full channel power is required to vaporize the coolant to satisfy the perfect gas law, and there is no excess power to raise the system pressure.

Expressions for the time of maximum pressure, t_m, and the maximum pressure, P_m, were derived by the approximate model, yielding

$$t_m = Km_0 \sqrt[3]{2\,Gbc^2/A^2q_1}, \tag{1}$$

and

$$P_m = K^* \sqrt[3]{2\,Gbq_i^2/A^2c} + P_0, \tag{2}$$

where m_0 is the initial coolant mass to be accelerated, G and b are calculated from material properties, c is the ratio of energy input to pressure rise for the system, A the channel cross-sectional area, q_1 the power, and P_0 the initial pressure. The computer problems solved previously led to values for K and K* of 1.27 and 0.75, respectively. With proportionality constants and the use of Eqs. (1) and (2), results from the computer were reproduced with maximum deviations of 17% and 10%, respectively. Ranges of parameters covered were: $0.866 \leq A^2 \leq 43.1$ cm^2; $5.86 \times 10^{11} \leq q_1 \leq 3.03 \times 10^{14}$ erg/sec; $34.8 \leq m_0 \leq 15{,}560$ gm; and $1.77 \leq c \leq 176.0$.

By a similar analysis, the ratio of kinetic energy at t_m to total system energy input was found to be proportional to the product of G and b. For the problems studied, this ratio was less than 5%. Hence, the neglect of kinetic energy in the energy balance equation used to derive both models should not seriously affect the accuracy.

4. Large TREAT Loop

The modified and repaired 4-in. P-K ball valves were shipped to the TREAT site in Idaho. Upon arrival, all of the crates housing the valves were found to be damaged to a large extent. Subsequent testing of these valves showed that none of the seal bellows leaked at 55 psig helium pressure, but all of the ball seats were reported as leaking. In addition, valve No. 15 leaked when a small head of water was placed above the ball, possibly due to the fact that the clearance between the guide pin and the ball was less than 0.0002 in. when the valve manual clearly sets this clearance as 0.0005 to 0.015 in. Furthermore, valve No. 14 exhibited an extremely jerky and unacceptable operation. A slight jerkiness is present in the remaining four valves. It is suspected that these conditions resulted from some structure misalignment during shipment.

Pipe expansion bellows are expected in approximately 40 days. Also, the 1- and 2-in. Fulton Sylphon control bellows and valves have been received and are being checked.

The cold trap components have been fabricated, and the unit is now approaching the assembly stage.

Calculations have been made pertinent to the force required to separate the header and pressure container after disassembly and removal of the test section. This figure is approximately 300 lb, which means precautions must be taken to insure that the Conoseal joints are free of sodium during disassembly.

Calculations also show that the pressure drop in the cold trap will be low (without oxide in the trap). The pressure drop will range from 0.66 psi to 2.0 psi at sodium flowrates of 20 and 60 gpm, respectively. These figures will rise to 1.19 and 3.57 psi with oxide in the trap. These figures indicate that bypass flow can be adequately maintained by operation of the main pump.

VI. PUBLICATIONS

Papers

HYDRIDE AND BIMETALLIC REGENERATIVE EMF CELLS
M. S. Foster, C. E. Johnson, A. K. Fischer, and C. E. Crouthamel
AMU-ANL Conference on Direct Energy Conversion, November 4-5, 1963. ANL-6802 (December 1963). pp. 53-63

FIRST OBSERVATION OF A SOLUTION OF Li_3Bi, AN INTERMETALLIC IN MOLTEN LITHIUM CHLORIDE AND LITHIUM CHLORIDE-LITHIUM FLUORIDE
M. S. Foster, C. E. Crouthamel, D. M. Gruen, and R. L. McBeth
J. Phys. Chem. 68, 980-981 (April 1964) Note

THE TRANSITIONAL BEHAVIOR OF THE MINIMUM CREEP RATE OF β-COBALT
J. E. Flinn and E. R. Gilbert
Phil. Mag. 9, 557-564 (April 1964)

THE SYSTEM URANIUM MONOPHOSPHIDE-URANIUM MONOSULPHIDE
P. D. Shalek and Y. Baskin
Bull. Amer. Cer. Soc. 43(4), 327 (April 1964) Abstract

SOLID SOLUTION IN THE SYSTEM URANIA-RARE EARTH OXIDE: I. UO_2-$GdO_{1.5}$
R. J. Beals and J. H. Handwerk
Bull. Amer. Cer. Soc. 43(4), 327 (April 1964) Abstract

TREAT STUDY OF THE PENETRATION OF MOLTEN URANIUM AND U-5 wt. % Fs ALLOY THROUGH TYPE 304 STAINLESS STEEL
C. M. Walter and C. E. Dickerman
Nucl. Sci. Eng. 18(4) 518-524 (April 1964)

RADIOGRAPHY AS A TOOL OF NONDESTRUCTIVE TESTING
Harold Berger
Proc. of the Symposium on Nondestructive Testing of Wood, Madison, Wisconsin, October 7-9, 1963. Forest Products Laboratory Report FPL-040 (March 1964). p. 16

PRESSURE TESTING OF THICK REINFORCED CONCRETE CELL
S. Fistedis
J. of the Structural Division, Proceedings ASCE, Vol. 90 (April 1964)

THE LIQUID METAL LINEAR GENERATOR
E. S. Sowa
AMU-ANL Conference on Direct Energy Conversion, November 4-5, 1963. ANL-6802 (December 1963). pp. 181-185

THERMIONIC ENERGY CONVERSION FOR DC AND HIGH FREQUENCY POWER OUTPUT
H. K. Richards
AMU-ANL Conference on Direct Energy Conversion, November 4-5, 1963. ANL-6802 (December 1963). pp. 152-160

WHY STUDY DIRECT CONVERSION?
B. I. Spinrad
AMU-ANL Conference on Direct Energy Conversion, November 4-5, 1963. ANL-6802 (December 1963). pp. 3-14

THICK TARGET NEUTRON YIELDS FOR 6 BeV PROTONS
J. W. Meadows, J. F. Whalen, and A. B. Smith
Bull. Am. Phys. Soc. 9(4), 460-461 (1964) Abstract

STATISTICAL THEORY OF NUCLEAR CROSS SECTIONS
P. A. Moldauer
Bull. Am. Phys. Soc. 9(4), 505 (1964) Abstract

CERTIFICATIONS OF ALGORITHMS 191 AND 192 HYPERGEOMETRIC AND CONFLUENT HYPERGEOMETRIC (A. P. Relph, Comm. ACM, July 1963)
H. C. Thacher
Comm. ACM 7(4), 244 (April 1964)

ELASTIC AND INELASTIC SCATTERING OF FAST NEUTRONS FROM Tl, Hg AND Au
W. G. Vonach, C. A. Engelbrecht, and A. B. Smith
Bull. Am. Phys. Soc. 9, 461 (April 1964) Abstract

ANL Reports

ANL-6271 SAFETY ANALYSIS REPORT, ARGONNE FAST CRITICAL FACILITY (ZPR-VI)
W. Y. Kato, G. J. Fischer, and L. R. Dates

ANL-6649 FABRICATION OF UO_2-STAINLESS STEEL DISPERSION FUEL FOR BORAX-V NUCLEAR SUPERHEAT
W. C. Kramer and C. H. Bean

ANL-6725 CHEMICAL ENGINEERING DIVISION SUMMARY REPORT, April, May, June, 1963

ANL-6796 THE SLUG-ANNULAR FLOW REGIME TRANSITION AT ELEVATED PRESSURE
Peter Griffith

ANL-6802 AMU-ANL CONFERENCE ON DIRECT ENERGY CONVERSION

ANL-6809 INTRODUCTORY FAST REACTOR PHYSICS ANALYSIS
David Meneghetti

ANL-6815 LABORATORY STUDIES OF IODINE BEHAVIOR IN THE EBR-II MELT REFINING PROCESS
N. R. Chellew, C. C. Honesty, and R. K. Steunenberg

ANL-6817 LABORATORY INVESTIGATIONS IN SUPPORT OF FLUID BED FLUORIDE VOLATILITY PROCESSES. PART VI. A. The Absorption Spectrum of Plutonium Hexafluoride. B. Analysis of Mixtures of Plutonium Hexafluoride and Uranium Hexafluoride by Absorption Spectrometry
Martin J. Steindler and William H. Gunther

ANL-6818 THE EBR-II SKULL RECLAMATION PROCESS. PART I. General Process Description and Performance
Leslie Burris, Jr., I. G. Dillon, and R. K. Steunenberg